than of exo*. Repulsions between the surface of platinum and the endo hydrogens of the endo* moieties are responsible for this additional destabilization.

4. *The reduction of (DO)PtR$_2$ complexes occurs via initial adsorption of the platinum atom in the organometallic complex.* We proposed this mechanism of adsorption in earlier papers[50-56] on the basis of the following: (1) the platinum atom is the most polarizable part of the complex; (2) it is incorporated into the surface of the catalyst; (3) stereochemical probes showed that the reduction of norbornadiene by D_2 incorporated deuterium predominantly into the exo positions of norbornane, but the similar reduction of (norbornadiene)dimethylplatinum(II) incorporated deuterium predominantly into the endo positions of norbornane. In this paper, we provide further stereochemical support for this conclusion with the observation that the reduction of homohypostrophene by D_2 incorporates deuterium exclusively into the exo positions of homohypostrophane, but similar reductions of **1** and **2** incorporate deuterium predominantly into the endo positions of homohypostrophane.

Acknowledgment. We thank Dr. Shaw Huang for assistance with the ^{2}H NMR experiments. We thank Watson Lees for assistance with the force field calculations and the 2D (COSY) ^{1}H NMR experiments.

Registry No. **1**, 131130-30-8; **2**, 131130-31-9; **3**, 51175-59-8; **4**, 2958-72-7; **5**, 54397-80-7; **6**, 112710-38-0; HOP, 30114-57-9; HOPH, 59015-02-0; (HOP)PtCl$_2$, 131130-32-0; (HOP)PtI$_2$, 135773-43-2; (HOP)PtNp$_2$, 131130-33-1; (HOP)Pt(Np)Cl, 131130-34-2; (HOP)Pt(Np)I, 131130-35-3; neopentylmagnesium chloride, 13132-23-5; *exo*-2-norbornylmagnesium bromide, 13058-86-1; *endo*-2-norbornylmagnesium bromide, 13058-87-2; *exo*-2-bromonorbornane, 2534-77-2; Zeise's dimer, 12073-36-8; cyclopentadiene, 542-92-7; benzoquinone, 106-51-4.

Supplementary Material Available: Details of the syntheses of homohypostrophene and its precursors (**3-6**) and the synthesis of neopentylmagnesium chloride and procedures for the determination of structure, summary of the crystallographic data, atomic coordinates and equivalent isotropic displacement parameters for non-hydrogen atoms, complete tables of bond distances and angles, anisotropic displacement parameters for non-hydrogen atoms, coordinates for hydrogen atoms, packing diagrams, and UV absorption spectra for **1** and **2** (24 pages); listing of observed and calculated structure factors for **1** and **2** (22 pages). Ordering information is given on any current masthead page.

Electrochemical Reduction of CO_2 Catalyzed by [Pd(triphosphine)(solvent)]$(BF_4)_2$ Complexes: Synthetic and Mechanistic Studies

Daniel L. DuBois,*,† Alex Miedaner,† and R. Curtis Haltiwanger‡

Contribution from the Solar Energy Research Institute, Golden, Colorado 80401, and Department of Chemistry and Biochemistry, University of Colorado, Boulder, Colorado 80309.
Received January 28, 1991. Revised Manuscript Received July 17, 1991

Abstract: The free radical addition of phosphorus-hydrogen bonds to carbon-carbon double bonds has been used to prepare a number of new tridentate ligands containing phosphorus. Reactions of these tridentate ligands with [Pd(CH$_3$CN)$_4$](BF$_4$)$_2$ yield the corresponding [Pd(tridentate)(CH$_3$CN)](BF$_4$)$_2$ complexes. These complexes catalyze the electrochemical reduction of CO_2 to CO in acidic dimethylformamide or acetonitrile solutions if the tridentate ligand is a linear triphosphine ligand. Complexes in which one or more of the phosphorus atoms of the tridentate ligand have been substituted with a nitrogen or sulfur heteroatom do not catalyze the electrochemical reduction of CO_2. Kinetic studies on [Pd(etpC)(CH$_3$CN)](BPh$_4$)$_2$ (where etpC is bis[(dicyclohexylphosphino)ethyl]phenylphosphine) show that, at acid concentrations above 1.0×10^{-2} M, the reaction is first order in catalyst, first order in CO_2, and independent of acid concentration. At acid concentrations less than 4.0×10^{-3} M, the catalytic rate is first order in catalyst, second order in acid, and independent of CO_2. The rate is also solvent dependent. A mechanism is proposed to account for these data. Comparison of the rate constants for catalysts with different alkyl and aryl substituents on the terminal phosphorus atoms indicates that the rate of reaction of the palladium(I) intermediates with CO_2 increases with the electron-donating ability of the R groups, and that steric interactions are of less importance. In contrast, the rate constants decrease with increasing steric bulk for substituents on the central phosphorus atoms of the triphosphine ligand. Other relationships between ligand structure and catalyst activity, selectivity, and stability are also discussed. An X-ray diffraction study of the catalytic decomposition product [Pd(etp)]$_2$(BF$_4$)$_2$ (where etp is bis[(diphenylphosphino)-ethyl]phenylphosphine) has been carried out. [Pd(etp)]$_2$(BF$_4$)$_2$ crystallizes in the monoclinic space group $P2_1/n$ with a = 13.842 (6) Å, b = 28.055 (8) Å, c = 19.596 (7) Å, β = 95.80 (3)°, v = 7571 (5) Å^3, and Z = 4. The structure was refined to R = 0.057 and R_w = 0.0809 for 10352 independent reflections ($F > 6\sigma(F)$). This Pd(I) dimer is bridged by two triphosphine ligands. A dihedral angle of 67° exists between the two nearly square planar PdP$_3$ fragments of [Pd(etp)]$_2$(BF$_4$)$_2$. This dimer can be reoxidized to regenerate the catalytically active complexes.

Introduction

The majority of homogeneous catalysts for the electrochemical reduction of CO_2 contain either nitrogen macrocycles[1-8] or bipyridine ligands.[9-13] A number of structurally characterized CO_2 complexes contain phosphine and arsine ligands,[14-16] and metal phosphine complexes catalyze a wide variety of homogeneous reactions.[17,18] However, there have been few reports of transition-metal phosphine complexes catalyzing the electrochemical

† Solar Energy Research Institute.
‡ University of Colorado.

(1) Collin, J.-P.; Sauvage, J.-P. *Coord. Chem. Rev.* **1989**, *93*, 245. This paper is an excellent review of the electrochemical reduction of carbon dioxide.
(2) Meshitsuka, S.; Ichikawa, M.; Tamaru, K. *J. Chem. Soc., Chem. Commun.* **1974**, 158.
(3) Fischer, B.; Eisenberg, R. *J. Am. Chem. Soc.* **1980**, *102*, 7363.
(4) Creutz, C.; Schwarz, H. A.; Wishart, J. F.; Fujita, E.; Sutin, N. *J. Am. Chem. Soc.* **1989**, *111*, 1153.

0002-7863/91/1513-8753$02.50/0

reduction of CO_2.[19-22] To develop this class of complexes further, we initiated a study of polyphosphine complexes of various transition metals as CO_2 reduction catalysts.[23,24] Polyphosphine ligands, as opposed to monodentate phosphine ligands, were chosen for study in an effort to prevent undesirable side reactions associated with phosphine ligand dissociation.[25-27] Also important to catalytic reactions is the generation of vacant sites for coordination of substrate molecules.[17,18] To incorporate this feature into the polyphosphine metal complexes, a series of complexes were synthesized that contained both polyphosphine and acetonitrile ligands. Dissociation of the weakly bound acetonitrile ligands could lead to formation of vacant coordination sites during a catalytic cycle. This approach led to the development of [Pd(triphosphine)L]$(BF_4)_2$ catalysts (where L is CH_3CN, PEt_3, PPh_3, or $P(OMe)_3$).[20,21] These results suggested that studies of palladium complexes containing various tridentate and monodentate ligands would contribute significantly to our understanding of factors important for catalytic activity and catalyst longevity. In this paper, the syntheses of a number of new tridentate ligands and their solvated palladium complexes [Pd(tridentate)(solvent)$(BF_4)_2$ are described. These complexes allow the effects of ligand parameters such as chain length, steric factors, phosphine basicity, and donor set to be studied. This has led to the development of better catalysts and a better mechanistic understanding of the catalytic reaction.

Experimental Section

Materials and Physical Methods. Details of methods used for drying solvents, spectral measurements, and gas chromatography experiments have been presented elsewhere.[20,23] The following reagents were purchased from commercial suppliers and used as obtained: divinylphenylphosphine, dimethylchlorophosphine, diethylphosphine, dicyclohexylphosphine, cyclohexylphosphine, 2,2'-azobis(2-methylproprionitrile) (AIBN), [$Pd_2(dba)_3$], and allylmagnesium bromide.

Coulometric measurements were carried out at 25–30 °C using a Princeton Applied Research Model 173 potentiostat equipped with a Model 179 digital coulometer and a Model 175 universal programmer. The working electrode was constructed from a reticulated vitreous carbon rod with a diameter of 1 cm and length of 2.5 cm (100 pores per inch, The Electrosynthesis Co., Inc.), the counter electrode was a Pt wire, and a silver wire coated with AgCl was used as a pseudoreference electrode.

Table I. Crystal Data and Data Collection Conditions and Solution and Refinement Details for [Pd(etp)]$_2(BF_4)_2$

empirical formula	$C_{73}H_{74}B_2F_8P_6Cl_6Pd_2$
color, habit	yellow parallelepipeds
crystal dimensions, mm	0.35 × 0.40 × 0.45
space group	monoclinic, $P2_1/n$
unit cell dimensions	
a, Å	13.842 (6)
b, Å	28.055 (8)
c, Å	19.596 (7)
β, deg	95.80 (3)
V, Å^3	7571 (5)
Z	4
d_{calcd}, g cm^{-3}	1.523
formula weight, amu	1736.3
absorption coefficient, mm^{-1}	0.867
radiation	Mo Kα (λ = 0.71073 Å)
temp, °C	−75
final residuals (obsd data), %	R = 5.70, R_w = 8.09
residuals (all data), %	R = 7.41, R_w = 9.25

The electrode compartments were separated by Vycor disks (7-mm diameter, EG&G Princeton Applied Research). Measurements of current efficiencies for gas production were carried out in a sealed flask from which aliquots were withdrawn for gas chromatographic (GC) analysis.[20] A number of detailed controlled potential electrolysis experiments are described under the appropriate compounds in the supplementary material. Typical electrolysis experiments required 1–4 h to complete and were carried out at potentials approximately 100 mV negative of the half-wave potentials given in Table IV. Catalytic coulometric experiments were considered complete when the current had decayed to approximately 10% of its original value in the presence of 0.18 M CO_2 and 0.1 M HBF_4, i.e., the same as the initial conditions. The initial concentration of catalyst was 1.0×10^{-3} M. Cyclic voltammetry and chronoamperometry experiments were carried out using a Cypress System computer-aided electrolysis system at 21 ± 0.5 °C unless stated otherwise. The working electrode was a glassy carbon electrode obtained from Bioanalytical Systems, Inc. The counter electrode and reference electrodes were as described above. Ferrocene was used as an internal standard, and all potentials are reported vs the ferrocene/ferrocenium couple. To obtain accurate values for peak currents to be used for i_p in the catalytic experiments, currents were measured on solutions containing the catalysts at concentrations between 1.0×10^{-3} and 6.0×10^{-3} M, under 1 atm of CO_2, and extrapolated to the lower concentrations used in the catalytic measurements. The solubility of CO_2 in dimethylformamide was taken from ref 28. All solutions for cyclic voltammetry and coulometric experiments were 0.3 N NEt_4BF_4 in dimethylformamide unless stated otherwise.

X-ray crystallographic measurements were carried out on a Siemens P3F autodiffractometer. Mo Kα radiation, monochromatized by diffraction of a highly oriented graphite crystal, was used for both studies. The crystals were mounted and coated with epoxy. Programs in the Siemens X-ray package were used for data collection and for structure solution and refinement. Details of the experimental conditions are given in the supplementary material. Table I summarizes the crystal data for [Pd(etp)]$_2(BF_4)_2$. Crystal data for [Pd(etpE)]$_2(BF_4)_2$ are given in the supplementary material.

Syntheses. Specific synthetic procedures are given in the following text for selected compounds. Detailed syntheses for all complexes and ligands are contained in the supplementary material.

Bis[(diethylphosphino)ethyl]phenylphosphine, etpE. A mixture of divinylphenylphosphine (3.25 g, 20 mmol), diethylphosphine (3.60 g, 40 mmol), and AIBN (100 mg) was irradiated in a sealed Schlenk flask using a Rayonet photoreactor with both 254- and 350-nm lamps for 1 day. Volatile materials were removed in vacuo at 25 °C (2 h). The remaining product (6.5 g, 95%) was used without further purification. ^{1}H NMR ($CDCl_3$): Ph, δ 7.3–7.5 (m); C_2H_5 and CH_2CH_2, δ 1.8–0.8 (complex multiplet).

[Pd(etpE)(CH_3CN)]$(BF_4)_2$. A solution of [$Pd(CH_3CN)_4$]$(BF_4)_2$[29,30] (4.44 g, 10 mmol) in acetonitrile (30 mL) was added via cannula to a stirred solution of etpE (3.42 g, 10 mmol) in dichloromethane (20 mL). The resultant red solution turned yellow within 2 min. After stirring for 1 h, the solvent was removed in vacuo at 50 °C for 1 h. Although this

(5) Beley, M.; Collin, J.-P.; Ruppert, R.; Sauvage, J.-P. *J. Am. Chem. Soc.* **1986**, *108*, 7461.
(6) Schmidt, H. M.; Miskelly, G. M.; Lewis, N. S. *J. Am. Chem. Soc.* **1990**, *112*, 3420.
(7) Becker, J. Y.; Vainas, B.; Eger, R.; Kaufman, L. *J. Chem. Soc., Chem. Commun.* **1985**, 1471.
(8) Kapusta, S.; Hackerman, N. *J. Electrochem. Soc.* **1984**, *131*, 1511.
(9) Hawecker, J.; Lehn, J. M.; Ziessel, R. *Helv. Chim. Acta* **1986**, *69*, 1990.
(10) Bolinger, C. M.; Story, N.; Sullivan, B. P.; Meyer, T. J. *Inorg. Chem.* **1988**, *27*, 4582.
(11) Ishida, H.; Tanaka, K.; Tanaka, T. *Organometallics* **1987**, *6*, 181.
(12) Daniele, S.; Ugo, P.; Bontempelli, G.; Floriani, M. *J. Electroanal. Chem.* **1987**, *219*, 259.
(13) Keene, F. R.; Creutz, C.; Sutin, N. *Coord. Chem. Rev.* **1985**, *64*, 247.
(14) Aresta, M.; Nobile, C. F.; Albano, V. G.; Forni, E.; Manassero, M. *J. Chem. Soc., Chem. Commun.* **1975**, *98*, 1615, 7405.
(15) Alvarez, R.; Camona, E.; Marin, J. M.; Poveda, M. L.; Cutierrez-Puebla, E.; Monge, A. *J. Am. Chem. Soc.* **1986**, *108*, 2286.
(16) Bristow, G. S.; Hitchcock, P.; Lappert, M. F. *J. Chem. Soc., Chem. Commun.* **1981**, 1145.
(17) Parshall, G. W. *Homogeneous Catalysis*; Wiley: New York, 1980.
(18) Masters, C. *Homogeneous Transition-Metal Catalysis*; Chapman and Hall: New York, 1981.
(19) Slater, S.; Wagenknecht, J. H. *J. Am. Chem. Soc.* **1984**, *106*, 5367.
(20) DuBois, D. L.; Miedaner, A. *J. Am. Chem. Soc.* **1987**, *109*, 113.
(21) DuBois, D. L.; Miedaner, A. In *Catalytic Activation of Carbon Dioxide*; Ayers, W. M., Ed.; ACS Symposium Series 363; American Chemical Society: Washington, DC, 1988; p 42.
(22) Milosavljevic, E. B.; Solujic, L.; Krassowski, D. W.; Nelson, J. H. *J. Organomet. Chem.* **1988**, *352*, 177.
(23) DuBois, D. L.; Miedaner, A. *Inorg. Chem.* **1986**, *25*, 4642.
(24) Miedaner, A.; DuBois, D. L. *Inorg. Chem.* **1988**, *27*, 2479.
(25) Bontempelli, G.; Magno, F.; Corain, B.; Schiavon, G. *J. Electroanal. Chem. Interfacial Electrochem.* **1979**, *103*, 243.
(26) Bontempelli, G.; Magno, F.; Corain, B. *Inorg. Chem.* **1981**, *20*, 2579.
(27) Jasinski, R. *J. Electrochem. Soc.* **1983**, *130*, 834.
(28) Stephen, H., Stephen, T., Eds. *Solubilities of Inorganic and Organic Compounds*; Pergamon Press: New York, 1958; Vol. 1, p 1063.
(29) Sen, A.; Ta-Wang, L. *J. Am. Chem. Soc.* **1981**, *103*, 4627.
(30) Hathaway, B. J.; Holah, D. G.; Underhill, A. E. *J. Chem. Soc.* **1962**, 2444.

material gave a satisfactory elemental analysis, it can be recrystallized from a mixture of dichloromethane and ethanol containing acetonitrile (approximately 5% by volume). The yield was 5.50 g (83%). Anal. Calcd for $C_{20}H_{36}NB_2F_8P_3Pd$: C, 36.21; H, 5.47; N, 2.11. Found: C, 36.46; H, 5.47; N, 2.05. ^{1}H NMR (CD_3NO_2): Ph, δ 7.7–8.7 (m); CH_2CH_2, δ 1.8–3.1 (m); C_2H_5, δ 1.0–1.5 (m); CH_3CN, δ 2.58 (s). IR: ν_{CN} 2295 (w), 2322 cm^{-1} (vw). Cyclic voltammetry and coulometry experiments are described in the text. The $E_{1/2}$ value obtained from catalytic experiments is −1.25 V.

[Pd(etpE)(PEt$_3$)](BF$_4$)$_2$. Triethylphosphine (0.15 mL, 1.0 mmol) was added via syringe to a solution of [Pd(etpE)(CH$_3$CN)](BF$_4$)$_2$ (0.66 g, 1.0 mmol) in dichloromethane (50 mL). After the reaction mixture was stirred for 1 h, ethanol (20 mL) was added to the solution, and the volume was reduced in vacuo to ~25 mL. The resulting yellow powder (0.65 g, 88%) was collected by filtration and dried in a vacuum at 50 °C for 5 h. Anal. Calcd for $C_{24}H_{48}B_2F_8P_4Pd$: C, 38.92; H, 6.55; F, 20.51. Found: C, 39.39; H, 6.80; F, 18.95. ^{1}H NMR (acetone-d_6): Ph, δ 7.8–8.5 (m); CH_2CH_2, δ 2.2–2.5 (m); C_2H_5, δ 0.9–1.6 (m). ^{31}P NMR (acetonitrile-d_3): PPh, 115.5 (dt, $J_{PPh-PEt_3}$ = 303 Hz, $J_{PPh-PEt_2}$ = 12 Hz); PEt_2, δ 55.9 (dd, $J_{PEt_2-PEt_3}$ = 30 Hz); PEt_3, δ 10.0 (dt). Cyclic voltammetry and coulometry experiments are described in the text.

[Pd(etpE)]$_2$(BF$_4$)$_2$. Method A. A solution of [Pd(CH$_3$CN)$_4$](BF$_4$)$_2$ (0.44 g, 1.0 mmol) in acetonitrile (30 mL) was added via a cannula to a solution of etpE (0.68 g, 2.0 mmol) in dichloromethane (50 mL). The mixture was stirred for 30 min, and then [Pd$_2$(dba)$_3$] (0.46 g, 0.5 mmol) was added as a solid. Stirring the initial suspension resulted in the formation of a clear red solution. The solvent was removed in vacuo, and the resulting solid was recrystallized from a mixture of dichloromethane and ethanol to yield yellow crystals (1.07 g, 79%). Anal. Calcd for $C_{36}H_{66}B_2F_8P_6Pd_2$: C, 40.35; H, 6.21. Found: C, 40.69; H, 6.27. ^{1}H NMR (CD_3CN): Three complex multiplets are observed at 7.3, 2.0, and 1.1 ppm. The resonance at 7.4 ppm is assigned to the phenyl group, and the resonances at 2.0 and 1.1 ppm are assigned to the ethyl and bridging methylene groups. ^{31}P NMR (CD_3CN): ABX pattern (see structure **6** of text): PhP, δ 61.1 (d, J = 350 Hz); Et_2P (trans to Pd), δ 40.9 (s); Et_2P (trans to P), δ 23.3 (d). All resonances have additional unresolved splitting. Electronic absorption spectrum: λ_{max} = 387 nm.

Method B. Controlled potential electrolysis of [Pd(etpE)(CH$_3$CN)](BF$_4$)$_2$ (0.025 g, 0.038 mmol) in THF was carried out at −1.5 V vs $FeCp_2$ using a reticulated vitreous carbon electrode. After the current had decayed to 4% of its initial value, the electrolysis was stopped. The charge passed was 3.86 C corresponding to 1.06 faradays/mol. The electronic spectrum and the ^{31}P NMR spectrum of the product were identical to those described previously for [Pd(etpE)]$_2$(BF$_4$)$_2$ prepared by method A. Cyclic voltammetry and coulometry experiments for this complex are discussed in the text.

Bis[(dicyclohexylphosphino)ethyl]phenylphosphine, etpC. A mixture of divinylphenylphosphine (4.62 g, 29 mmol), dicyclohexylphosphine (11.3 g, 57 mmol), and AIBN (0.1 g) was irradiated in a Schlenk flask for 2 days. Volatile materials were removed in vacuo at 150 °C. The crude product (13.25 g, 82%) was used without further purification. ^{1}H NMR (toluene-d_8): Ph, δ 7.1, 7.5 (m); CH_2CH_2, C_6H_{11}, δ 1.2, 1.6 (m).

[Pd(etpC)(CH$_3$CN)](BPh$_4$)$_2$. A solution of [Pd(CH$_3$CN)$_4$](BF$_4$)$_2$ (2.22 g, 5 mmol) in acetonitrile (30 mL) was added via cannula to a stirred solution of etpC (2.79 g, 5 mmol) in dichloromethane (20 mL). The yellow reaction mixture was stirred for 1 h, and the solvent was removed under vacuum. The resulting yellow solid was washed with hexanes and dried (3.90 g, 88%). An analytic sample was obtained by dissolving the crude [Pd(etpC)(CH$_3$CN)](BF$_4$)$_2$ (2.0 g, 2.27 mmol) in dichloromethane (20 mL) containing acetonitrile (1 mL). To this solution was added a second solution containing sodium tetraphenylborate (2.8 g) in a mixture of acetone (40 mL) and ethanol (20 mL). The volume of the resulting solution was reduced in vacuo to approximately 30 mL. The resulting microcrystalline solid was collected by filtration and dried in a vacuum at 70 °C for 2 h (2.54 g, 1.89 mmol, 83% recovery). Anal. Calcd for $C_{84}H_{100}NB_2P_3Pd$: C, 75.03; H, 7.50; N, 1.04. Found: C, 74.74; H, 7.52; N, 1.09. ^{1}H NMR (CD_3NO_2): Ph, δ 7.6–7.8 (m); CH_2CH_2, δ 3.4 (m) and 2.5–2.7 (m); CH_3CN, δ 2.54 (s); cyclohexyl, δ 1.0–1.8 (m). IR: ν_{CN} 2285 (w), 2310 cm^{-1} (vw). Cyclic voltammograms exhibit an irreversible cathodic wave at −1.36 V with an associated irreversible anodic wave at −0.99 V. A value of −1.28 V was determined for $E_{1/2}$ of the II/I couple. This value is based on the half-wave potential observed for the catalytic reduction of CO_2. Controlled potential electrolysis of [Pd(etpC)(CH$_3$CN)](BF$_4$)$_2$ (42 mg, 0.048 mmol) in dimethylformamide (10 mL) at −1.5 V vs $FeCp_2$ resulted in the passage of 4.78 C corresponding to 1.0 faradays/mol.

[Pd(ttp)H](BF$_4$). A solution of [Pd(ttp)P(OMe)$_3$][20] (0.95 g, 1.2 mmol) in acetonitrile (50 mL) was added to a solution of NH_4PF_6 (2.0 g, 12 mmol) in acetonitrile (30 mL), and the reaction mixture was stirred for 1 h. The solvent was removed in vacuo to produce a yellow powder, which was washed with water (50 mL) and dried at 50 °C under vacuum for 5 h (yield 0.78 g, 74%). The product may be recrystallized from a mixture of dichloromethane and ethanol, but analytically pure samples were not obtained. IR (Nujol): Pd–H stretch 1885 cm^{-1}. ^{1}H NMR (acetonitrile-d_3): PdH, δ −4.2 (dt, trans J_{PH} = 199 Hz, cis J_{PH} = 17 Hz); propylene protons, δ 1.8–2.6 (m); Ph, δ 7.5 (m). ^{31}P NMR (acetonitrile-d_3): Ph_2P, δ −14.9 (t, J = 46 Hz); PhP, δ 10.7 (d).

[Pd(etp)]$_2$(BF$_4$)$_2$. A solution of [Pd(CH$_3$CN)$_4$](BF$_4$)$_2$ (0.44 g, 1.0 mmol) in acetonitrile (30 mL) was added to a solution of etp (etp is bis[(diphenylphosphino)ethyl]phenylphosphine; 1.08 g, 2.0 mmol) in dichloromethane (50 mL). The resulting orange solution was stirred for 1 h, and then [Pd$_2$(dba)$_3$] (0.92 g, 0.5 mmol) was added. A clear red solution formed within 30 min, which was stirred for an additional 1 h. The solvent was removed in vacuo to produce a yellow solid. Crystals suitable for an X-ray diffraction study were obtained by recrystallization from a mixture of dichloromethane and ethanol (1.30 g, 90%). Anal. Calcd for $C_{68}H_{66}B_2F_8P_6Pd_2$: C, 56.11; H, 4.58. Found: C, 55.84; H, 4.55. ^{1}H NMR (acetonitrile-d_3): Ph, δ 6.6–7.7 (m); CH_2CH_2, δ 2.4–2.8 (m). ^{31}P NMR (acetonitrile-d_3): ABX spectrum: PhP, δ 59.3 (d, J = 326 Hz); Ph_2P (trans to Pd), δ 39.7 (s), Ph_2P (trans to PhP), δ 24.4 (d). All reasonances have additional unresolved splitting. Electronic absorption spectrum: λ_{max} = 420 nm. A cyclic voltammogram of [Pd(etp)]$_2$(BF$_4$)$_2$ in acetonitrile exhibits an irreversible cathodic wave at −1.53 V with an associated anodic wave at −0.88 V. An irreversible oxidation wave is observed at +0.82 V.

Results

Synthetic Studies. The free radical addition of the phosphorus–hydrogen bond to carbon–carbon double bonds of vinyl and allyl groups[31-33] has been used to prepare a variety of new triphosphine ligands as shown in reactions 1 and 2.[34] These reactions

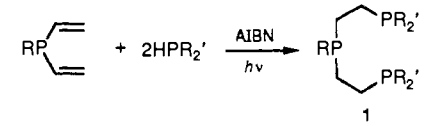

(1)

1

1	R	R'
etp	Ph	Ph
etpE	Ph	Et
etpC	Ph	Cy
MetpE	Me	Et
MetpC	Me	Cy
BetpN	*t*-Bu	neopentyl
NetpN	neopentyl	neopentyl
BetpE	*t*-Bu	Et

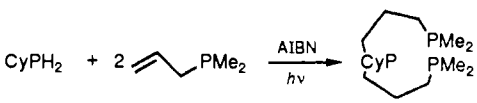

(2)

CitpM, **2**

can be readily followed by ^{31}P and ^{1}H NMR. The reactions of vinylphosphines with secondary phosphines (reaction 1) are nearly quantitative.[32] When the alkyl groups become extremely bulky, the reactions are slower and less quantitative. For example, when R is phenyl and R′ is ethyl, the reaction is complete within 2 or 3 h. When R is *tert*-butyl and R′ is neopentyl, reaction 1 requires 2 days to reach completion, and the yield is lower. When R and R′ are both *tert*-butyl, no reaction is observed. In the latter case, the bulkiness of the *tert*-butyl groups completely inhibits the reaction. As shown in eq 2, the reaction of primary phosphines with allylphosphines can also be used to prepare triphosphine ligands. This reaction is generally slower and results in more side products than are observed in reaction 1 for vinylphosphines.[33,35]

(31) Uriarte, R.; Mazanec, T. J.; Tau, K. D.; Meek, D. W. *Inorg. Chem.* **1980**, *19*, 79.
(32) DuBois, D. L.; Myers, W. H.; Meek, D. W. *J. Chem. Soc., Dalton Trans.* **1975**, 1011.
(33) Hietkamp, S.; Lebbe, T.; Spiegel, G. U.; Stelzer, O. *Z. Naturforsch.* **1987**, *42b*, 177.
(34) The ligand etp is commercially available. The ligand NetpN has been prepared previously using King's base-catalyzed method. King, R. B.; Cloyd, J. C., Jr.; Reimann, R. H. *J. Org. Chem.* **1976**, *41*, 972. The synthesis described here eliminates several steps.
(35) Arpac, E.; Dahlenburg, L. *Angew. Chem., Int. Ed. Engl.* **1982**, *21*, 931.

Table II. ^{31}P NMR Data of Ligands and $[Pd(L)(CH_3CN)](BF_4)_2$ Complexes

	ligands, L[a]			$[Pd(L)(CH_3CN)](BF_4)_2$ complexes[b]		
L	δ_C(calcd)[c]	δ_T(calcd)[c]	J, Hz	$\delta_C(\Delta_C)$	$\delta_T(\Delta_C)$	J, Hz
etp	−16.6 (−16)	−12.8 (−12)	29	116.4 (133)	54.6 (67)	7.3
etpE	−16.4 (−16)	−17.9 (−20)	24	114.1 (131)	61.9 (80)	7.3
etpC	−16.8 (−16)	−0.8 (0)	24	115.6 (132)	74.5 (75)	3.9
MetpE	−34.7 (−34)	−20.2 (−20)	20	105.5 (140)	62.3 (82)	5
MetpC	−33.6 (−34)	−1.0 (0)	22	107.8 (141)	75.8 (77)	~0
NetpN	−31.4 (−31)	−43.7 (−42)	20	110.0 (141)	46.2 (90)	~0
BetpN	5.8 (6)	−43.1 (−42)	24	139.5 (134)	51.9 (95)	~0
BetpE	6.9 (6)	−19.4 (−20)	22	142.0 (135)	65.7 (85)	~0
ttp	−29.0 (−28)	−18.0 (−18)	>1	1.14 (30)	−5.2 (13)	24
CttpM	−21.6 (−22)	−54.7 (−54)	>1	10.4 (32)	−19.1 (36)	27
PPS	−22.0 (−24)	−13.6 (−12)	29	116.9 (139)	63.3 (77)	4
PPy_2	−24.0 (−22)			47.0 (71)		

[a] All spectra were recorded in toluene-d_8 or chloroform-d_1. δ_C and δ_T are the chemical shifts of the central and terminal phosphorus atoms of the tridentate ligands. All chemical shifts are referenced to external H_3PO_4. [b] All spectra were recorded in acetonitrile-d_3. [c] Chemical shift values in parentheses were calculated using eq 2-1 and the aryl and alkyl group contributions of ref 36. Alkyl group values of 14, 8, 6, and 3 were used for CH_2CH_2P, $CH_2CH_2CH_2P$, CH_2CH_2SPh, and neopentyl groups, respectively. These values are based on the chemical shifts reported in refs 31 and 32 for compounds containing these functional groups.

Two new tridentate ligands containing mixed donor sets were prepared as shown in reactions 3 and 4. These two reactions illustrate the usefulness of this reaction for preparing ligands containing donors other than phosphorus.[32]

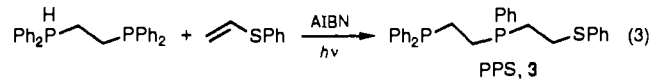

PPS, 3

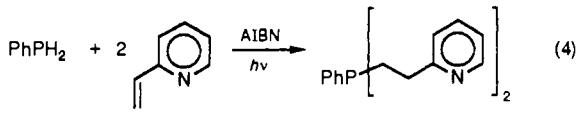

PPY, 4

The ^{31}P NMR data for the tridentate ligands are listed in Table II. The phosphorus–phosphorus coupling constants for the ligands containing an ethylene linkage are between 20 and 30 Hz. This coupling is less than 1 Hz for ttp and CttpM, which contain trimethylene linkages. The chemical shifts of the different phosphorus nuclei listed in Table II can be calculated using empirically determined alkyl group contributions.[36] The calculated chemical shifts shown in parentheses are typically within 2 ppm of the experimental values. These data provide confirmation of the identity of the triphosphine ligands. The ^1H NMR spectra (see Experimental Section and supplementary material) and the characterization of metal derivatives of each of the ligands also support their formulations.

Reaction of tridentate ligands with $[Pd(CH_3CN)_4](BF_4)_2$ provides a convenient route to complexes of the type [Pd(tridentate)$(CH_3CN)](BF_4)_2$ (reaction 5). This approach is more direct than the conventional approach of preparing halide complexes followed by halide abstraction using silver or thallium reagents. These complexes are usually yellow or white, stable to oxygen, and somewhat hygroscopic. They have been characterized by ^1H and ^{31}P NMR spectroscopy, IR spectroscopy, and elemental analyses.

$$[Pd(CH_3CN)_4](BF_4)_2 + \text{tridentate} \rightarrow [Pd(\text{tridentate})(CH_3CN)](BF_4)_2 + 3CH_3CN \quad (5)$$

5

The ^{31}P NMR spectra of complexes with triphosphine ligands containing ethylene linkages consist of a doublet and a triplet with a coupling constant of 0–12 Hz. Complexes with triphosphine ligands containing a trimethylene backbone exhibit larger coupling constants of approximately 25 Hz. Another significant difference between these two classes of compounds is the coordination chemical shift, Δc, (calculated as the chemical shift of the free ligand minus the chemical shift of the coordinated ligand) of the central phosphorus atom of the tridentate ligand. For complexes with an ethylene linkage, Δc is approximately 130–140 ppm, and for the trimethylene linkage Δc is close to 30 ppm. This difference in coordination chemical shifts has been observed previously for other metal complexes and provides a useful method for determining ring size.[37] The fact that Δc is 139 ppm for acetonitrile solutions of $[Pd(PPS)(CH_3CN)](BF_4)_2$ provides strong evidence that the sulfur atom is coordinated to palladium. All of the complexes in Table II that contain a coordinated acetonitrile ligand exhibit a resonance assigned to coordinated acetonitrile at approximately 2.5 ppm in their ^1H NMR spectra in noncoordinating solvents (see Experimental Section and supplementary material). Two bands are also observed in the infrared spectra of the acetonitrile complexes at approximately 2290 and 2310 cm^{-1}. The band at approximately 2290 cm^{-1} is assigned to the CN stretch of coordinated acetonitrile. The weak absorption at approximately 2310 cm^{-1} is assigned to a combination band.[23,38]

The acetonitrile ligands of the $[Pd(\text{tridentate})(CH_3CN)](BF_4)_2$ complexes are readily substituted. For example, the reaction of $[Pd(etpE)(CH_3CN)](BF_4)_2$ with triethylphosphine, trimethylphosphite, or chloride results in the formation of $[Pd(etpE)(PEt_3)](BF_4)_2$, $[Pd(etpE)P(OMe)_3](BF_4)_2$, and [Pd(etpE)Cl]$(BF_4)$, respectively. The lability of the acetonitrile ligand is demonstrated by the observation that the addition of small amounts of acetonitrile to solutions of $[Pd(\text{tridentate})(CH_3CN)](BF_4)_2$ complexes in noncoordinating solvents such as deuteriodichloromethane or deuterionitromethane results in a single acetonitrile resonance with a chemical shift between free and coordinated acetonitrile. This result confirms a rapid exchange between free and coordinated acetonitrile. In dimethylformamide (DMF) and dimethyl sulfoxide (DMSO), ^1H NMR resonances are observed for free acetonitrile. This indicates that acetonitrile is readily displaced by these solvents. As expected from these observations, the recrystallization of $[Pd(terpyridine)(CH_3CN)](BF_4)_2$ from a mixture of dimethylformamide and diethyl ether resulted in the formation of $[Pd(terpyridine)(DMF)](BF_4)_2$.

The hydride complex $[Pd(ttp)H](BF_4)$ was prepared by chemical reduction of $[Pd(ttp)P(OMe)_3](BF_4)_2$ to $[Pd(ttp)P(OMe)_3]$ followed by protonation with NH_4PF_6. The proton NMR spectrum of this hydride exhibits a doublet of triplets at 4.2 ppm upfield from TMS. A Pd–H stretch is observed at 1885 cm^{-1} in the infrared spectrum. The ^{31}P and ^1H NMR spectra for this complex indicate a purity greater than 90%; however, we were unable to obtain satisfactory elemental analyses for this complex. Reaction of $[Pd(ttp)H](BF_4)$ with HBF_4 in acetonitrile resulted in the formation of hydrogen and $[Pd(ttp)(CH_3CN)](BF_4)_2$. No reaction is observed between $[Pt(ttp)H](BF_4)_2$ and CO_2.

(36) Fluck, E.; Heckmann, G. In *Phosphorus-31 NMR Spectroscopy in Stereochemical Analysis*; Verkade, J. G., Quin, L. D., Eds.; Methods in Stereochemical Analysis Series No. 8; VCH: Deerfield Beech, 1987; pp 88–93.

(37) Garron, P. E. *Chem. Rev.* **1981**, *81*, 229.

(38) Storhoff, B. N.; Lewis, C. H., Jr. *Coord. Chem. Rev.* **1977**, *33*, 1.

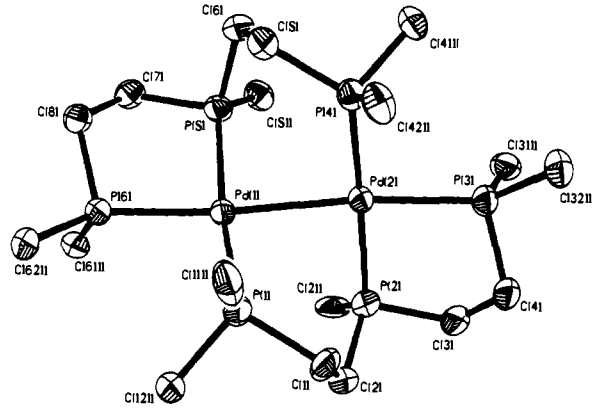

Figure 1. Drawing of $[Pd(etp)]_2^{2+}$ cation showing the atom numbering scheme.

Electrochemical reductions of $[Pd(etp)(CH_3CN)](BF_4)_2$ and $[Pd(etpE)(CH_3CN)](BF_4)_2$ lead to the formation of Pd(I) dimers **6a** and **6b**. These same complexes, which are also formed during catalyst deactivation, can be prepared by the reaction of 1 mol of $[Pd(triphosphine)(CH_3CN)](BF_4)_2$ with 0.5 mol of $[Pd_2(dba)_3]$ (where dba is bis(dibenzylidene)acetone) and 1 mol of the appropriate triphosphine ligand as shown in eq 6. The ^{31}P NMR

$$\tfrac{1}{2}[Pd_2(dba)_3] + \begin{matrix}PR_2'\\ |\\ RP-Pd-NCCH_3\\ |\\ PR_2'\end{matrix}^{2+} + RP(CH_2CH_2PR'_2)_2 \longrightarrow \begin{matrix}R_2'P & PR\\ | & |\\ R_2'P-Pd-Pd-PR_2'\\ | & |\\ R & PR_2'\end{matrix}^{2+} \quad (6)$$

6a, R = Ph, R' = Ph
6b, R = Ph, R' = Et

spectra of **6a** and **6b** each exhibit five-line patterns. The five-line patterns consist of an AB quartet which arises from the strong trans coupling between PR and PR_2'. The fifth line is assigned to the resonance of the PR_2' group trans to the palladium–palladium bond. Although additional splitting of each of the five lines is observed, the splitting is not sufficiently resolved to allow more complete analyses of the spectra. An intense absorption band at approximately 400 nm is also observed in the electronic absorption spectra of these complexes. This band appears to be associated with the presence of a palladium–palladium bond.

Structural Studies. X-ray diffraction studies of $[Pd(etp)]_2(BF_4)_2$ and $[Pd(etpE)]_2(BF_4)_2$ were carried out to confirm the structures suggested by ^{31}P NMR data. Yellow crystals of $[Pd(etp)]_2(BF_4)_2$ and $[Pd(etpE)]_2(BF_4)_2$ suitable for structure determinations were grown from mixtures of dichloromethane and ethanol. Crystals of $[Pd(etp)_2]_2(BF_4)$ consist of $[Pd(etp)]_2^{2+}$ cations, BF_4 anions, and three dichloromethane solvent molecules. A drawing of the cation is shown in Figure 1. This drawing illustrates the dimeric structure of the cation and the presence of two bridging triphosphine ligands. Selected bond distances and angles for the $[Pd(etp)_2]^{2+}$ cation are shown in Table III. The Pd–Pd bond length of 2.62 Å is comparable to that of other structurally characterized palladium(I) and platinum(I) dimers.[39-43] The

Table III. Selected Bond Lengths (Å) and Bond Angles (deg) for $[Pd(etp)]_2(BF_4)_2$

Bond Lengths			
Pd(1)–Pd(2)	2.617 (1)	Pd(1)–P(1)	2.305 (2)
Pd(1)–P(5)	2.308 (2)	Pd(1)–P(6)	2.358 (2)
Pd(2)–P(2)	2.327 (2)	Pd(2)–P(3)	2.355 (2)
Pd(2)–P(4)	2.323 (2)		
Bond Angles			
Pd(2)–Pd(1)–P(1)	85.9 (1)	Pd(2)–Pd(1)–P(5)	88.8 (1)
P(1)–Pd(1)–P(5)	167.3 (1)	Pd(2)–Pd(1)–P(6)	173.6 (1)
P(1)–Pd(1)–P(6)	100.1 (1)	P(5)–Pd(1)–P(6)	84.8 (1)
Pd(1)–Pd(2)–P(2)	88.6 (1)	Pd(1)–Pd(2)–P(3)	173.1 (1)
P(2)–Pd(2)–P(3)	84.5 (1)	Pd(1)–Pd(2)–P(4)	88.4 (1)
P(2)–Pd(2)–P(4)	172.2 (1)	P(3)–Pd(2)–P(4)	98.3 (1)

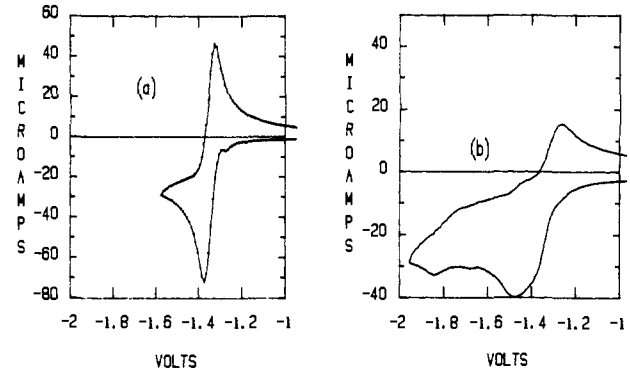

Figure 2. (a) Cyclic voltammogram of 3.1×10^{-3} M $[Pd(etpE)(PEt_3)](BF_4)_2$. (b) Cyclic voltammogram of 3.0×10^{-3} M $[Pd(etpE)(DMF)](BF_4)_2$. The solutions were 0.3 N NEt_4BF_4 in dimethylformamide, and the working electrode was glassy carbon. The scan rates were 50 mV/s for (a) and 100 mV/s for (b).

Pd–P bond lengths, which range from 2.30 to 2.35 Å, are also normal. The average Pd–P distance for the two bonds trans to palladium is 2.356 Å. This value is larger than the average Pd–P distance of 2.316 Å observed for the four Pd–P bonds trans to phosphorus atoms. This result suggests that the trans influence of palladium is greater than that of phosphorus, consistent with previous observations.[24,44] The lack of planarity of the ligands in the coordination sphere of each of the palladium atoms is indicated by the fact that the trans P–Pd–P and P–Pd–Pd angles of Pd(1) and Pd(2) are approximately 10° less than 180°. The two bridging triphosphine ligands form two five-membered rings containing one palladium atom and two six-membered rings containing two palladium atoms. The ring strain present in the five-membered rings is reflected in the average P–Pd–P angle of 84.6° compared to an ideal 90° angle. This strain is relieved somewhat when the ligand bridges the two palladium atoms. The average P–Pd–Pd angle for the two six-membered rings is 87.9°. The two P–Pd–P angles that are not part of a ring, P(1)–Pd(1)–P(6) and P(3)–Pd(2)–P(4), have an average value of 99.2°. These larger angles are required to compensate for the smaller angles observed in the ring systems.

The $[Pd(etpE)]_2^{2+}$ cation has the same basic structure as the $[Pd(etp)]_2^{2+}$ cation with two bridging triphosphine ligands and a palladium–palladium bond (see supplementary material). Both of these dimers consist of two approximately square planar molecules joined by Pd–Pd bonds. The dihedral angle between the best fit planes of these two square-planar units for $[Pd(etp)]_2^{2+}$ is 67°. Similarly for $[Pd(etpE)]_2^{2+}$ the dihedral angle between the best fit plane of Pd(1) and its four ligands and the best fit plane defined by Pd(2) and its four ligands is 68°. The observation that the dihedral angles of $[Pd(etp)]_2^{2+}$ and $[Pd(etpE)]_2^{2+}$ are nearly the same suggests that this angle is determined largely by the six-membered ring of the bridging ligand. Structures of

(39) Colton, R.; McCormick, M. J.; Pannan, C. D. *Aust. J. Chem.* **1978**, *31*, 1425.
(40) Fisher, J. R.; Mills, A. J.; Brown, M. P.; Thomson, M. A.; Puddephatt, R. J.; Frew, A. A.; Manojlovic-Muir, L.; Muir, K. W. *Organometallics* **1982**, *1*, 1421.
(41) Blau, R. J.; Espenson, J. H.; Kim, S.; Jacobson, R. A. *Inorg. Chem.* **1986**, *25*, 757.
(42) Manojlovic-Muir, L.; Muir, K. W. *J. Organomet. Chem.* **1981**, *219*, 129.
(43) Manojlovic-Muir, L.; Muir, K. W.; Lloyd, B. R.; Puddephatt, R. J.; Rashidi, M. *Inorg. Chim. Acta* **1977**, *23*, L33.
(44) Blau, R. J.; Espenson, J. H. *Inorg. Chem.* **1986**, *25*, 878.

palladium and platinum dimers containing two bridging bis(diphenylphosphino)methane ligands, which have five-membered rings, typically exhibit dihedral angles of approximately 40°.[39-43] Dimers with no bridging ligands exhibit a wide range of angles between 60° and 90°.[45-48] It appears that the ring size of the bridging chelating ligand can be used to control the dihedral angle of the palladium(I) dimers. This dihedral angle will likely have a major influence on the chemistry observed for these dimers since it controls the overlap of various fragment orbitals.

Electrochemical Studies. The electrochemical properties of the [Pd(tridentate)L]$(BF_4)_2$ complexes are dependent on both the nature of the tridentate ligand and L. Cyclic voltammograms of [Pd(etpE)L]$(BF_4)_2$ complexes are shown in Figure 2 for L equal to triethylphosphine and dimethylformamide (traces a and b, respectively). When L is triethylphosphine (Figure 2a), a diffusion-controlled, reversible, two-electron reduction is observed at −1.35 V versus the ferrocene/ferrocenium couple. The reduction wave has a peak-to-peak separation of 35 mV and an i_{pa}/i_{pc} ratio of 1.0 at a scan rate of 20 mV/s. These data are consistent with a reversible, two-electron process for which a peak-to-peak separation of 30 mV and an i_{pa}/i_{pc} ratio of 1.0 are expected. Linear plots of i_{pa} and i_{pc} versus $\nu^{1/2}$ from 20 to 400 mV/s indicate a diffusion-controlled process.[49] Controlled potential electrolysis at −1.45 V resulted in the passage of 1.9 faradays of charge/mol of complex. A cyclic voltammogram recorded on the reduced solution exhibited an oxidation wave at −1.35 V. These results demonstrate a chemically reversible and an electrochemically reversible two-electron process. Thus, when L is a phosphine ligand, a reversible two-electron reduction is observed. These results are similar to those reported previously for [Pd(etp)(PR_3)]$(BF_4)_2$ complexes.[20,21]

A cyclic voltammogram of [Pd(etpE)(DMF)]$(BF_4)_2$ (generated by dissolving [Pd(etpE)(CH_3CN)]$(BF_4)_2$ in dimethylformamide is shown in Figure 2b. Two cathodic waves and one anodic wave are observed. The broad cathodic wave with a peak at −1.48 V is diffusion controlled as indicated by linear i_p versus $\nu^{1/2}$ plots. The ratio of the peak current for this wave compared to that of [Pd(etpE)(PEt_3)]$(BF_4)_2$ under identical conditions is 0.38. Although this ratio is consistent with a one-electron process for which a value of 0.35 is expected,[50] the observation that $E_p - E_{p/2}$ is 135 mV suggests the possibilitty of two overlapping one-electron waves. This is supported by differential pulse voltammograms which exhibit a peak at −1.36 V and a shoulder at −1.46 V. Linear chronocoulometric plots of charge versus $t^{1/2}$ have nearly identical slopes for [Pd(etpE)(DMF)]$(BF_4)_2$ and [Pd(etpE)(PEt_3)]$(BF_4)_2$ ((slope of DMF complex)/(slope of PEt_3 complex) = 0.97). This indicates that the number of electrons transferred during the potential step (from approximately 200 mV positive of the onset of the cathodic waves to approximately 100 mV past the peak of the waves) is the same for these two compounds.[51] Since [Pd(etpE)(PEt_3)]$(BF_4)_2$ undergoes a two-electron reduction, two electrons are also transferred to [Pd(etpE)(DMF)]$(BF_4)_2$ when the potential is stepped across the cathodic wave shown in Figure 2b. The broad cathodic wave at −1.48 V in the cyclic voltammogram is, therefore, assigned to two one-electron reductions. This indicates the presence of a distinct Pd(I) intermediate that can be intercepted by reaction with CO_2 as discussed below for [Pd(etpC)(DMF)]$(BF_4)_2$.

Controlled potential electrolysis of [Pd(etpE)(DMF)]$(BF_4)_2$ at −1.65 V results in the passage of 1.0 faradays of charge/mol of complex and the formation of [Pd(etpE)]$_2(BF_4)_2$. The product was identified by ^{31}P NMR spectroscopy, electronic absorption spectroscopy, and cyclic voltammetry. These results indicate that on the time scale of the chronocoulometric experiment (approximately 1 s) a two-electron reduction product is formed at −1.65 V, but a one-electron product is formed on the longer time scale of the electrolysis experiment. The very small cathodic wave at −1.86 V in Figure 2b is assigned to the dimer [Pd(etpE)]$_2(BF_4)_2$, which forms subsequent to the reduction at −1.48 V. As the scan rate is increased, this wave becomes relatively smaller. Reversal of the direction of the scan immediately after traversing the peak at −1.48 V shows that the anodic wave at −1.27 V is coupled to the wave at −1.48 V. This wave is tentatively assigned to [Pd(etpE)].

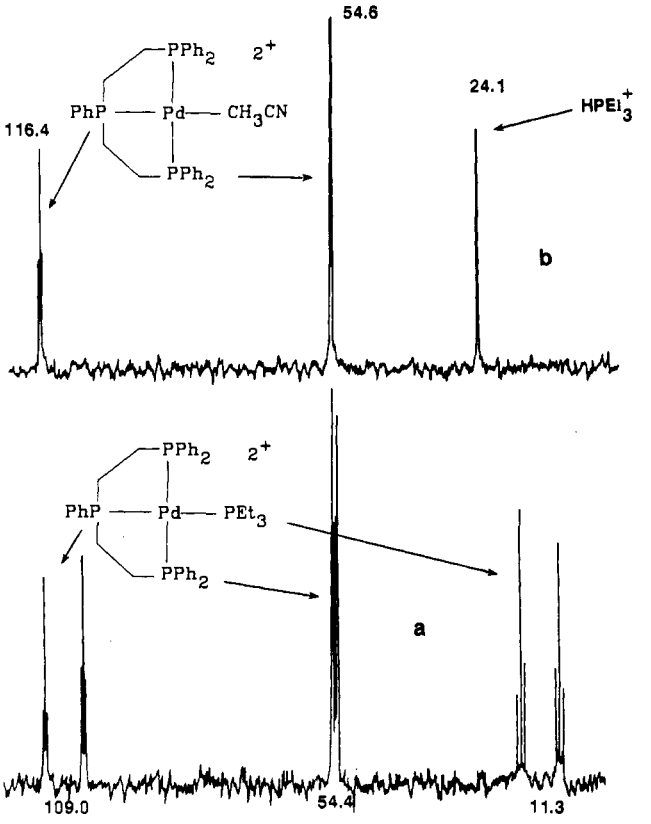

Figure 3. (a) ^{31}P NMR spectrum of [Pd(etp)(PEt_3)]$(BF_4)_2$ in acetonitrile-d_3. (b) Spectrum of the same solution after adding HBF_4 ([HBF_4] = 3×10^{-2} M).

From this data, it can be seen that the nature of the monodentate ligand can determine the electrochemical reversibility of the electrochemical reductions of [Pd(etpE)L]$(BF_4)_2$ complexes and whether a single two-electron reduction or two closely spaced, one-electron reductions are observed. The electrochemical behavior of [Pd(etpE)(CH_3CN)]$(BF_4)_2$ is typical of most of the [Pd(triphos)(CH_3CN)]$(BF_4)_2$ complexes. However, for Pd(ttp)(CH_3CN)]$(BF_4)_2$, [Pd(BetpN)(CH_3CN)]$(BF_4)_2$, and [Pd(NetpN)(CH_3CN)]$(BF_4)_2$, the reduction waves are somewhat more reversible and exhibit prewaves resulting from adsorption of palladium(0) complexes on the electrode.

The cyclic voltammogram of [Pd(etpE)]$_2(BF_4)_2$ in acetonitrile exhibits an irreversible diffusion-controlled cathodic wave at −1.86 V with associated irreversible anodic waves at −1.63 V (unassigned) and −1.25 V assigned to [Pd(etpE)]. Controlled potential electrolysis at −2.1 V in tetrahydrofuran resulted in the passage of 1.8 faradays of charge/mol of dimer. A third anodic wave at +0.58 V is also irreversible and diffusion controlled. Oxidation at +0.75 V in acetonitrile resulted in the passage of 2.0 faradays/mol of dimer and the formation of [Pd(etpE)(CH_3CN)]$(BF_4)_2$. The identity of the product was determined by ^{31}P NMR spectroscopy and cyclic voltammetry. From these results, it is clear that reduction of [Pd(etpE)(CH_3CN)]$(BF_4)_2$ to [Pd-

(45) Al-Resayes, S. I.; Hitchcock, P. B.; Nixon, J. F. *J. Organomet. Chem.* **1984**, *267*, C13.
(46) Jarchow, O.; Schultz, H.; Nast, R. *Angew. Chem., Int. Ed. Engl.* **1970**, *9*, 71.
(47) Doonan, D. J.; Balch, A. L.; Goldberg, S. Z.; Eisenberg, R.; Miller, J. S. *J. Am. Chem. Soc.* **1975**, *97*, 1961.
(48) Modinos, A.; Woodward, P. *J. Chem. Soc., Dalton Trans.* **1975**, 1516.
(49) Bard, A. J.; Faulkner, L. R. *Electrochemical Methods*; Wiley: New York, 1980; p 218.
(50) Andrieux, C. P.; Saveant, J. M In *Investigation of Rates and Mechanisms of Reactions*; Bernasconi, C. F., Ed.; Wiley: New York, 1986; Vol. 6, 41E, Part 2, pp 330–333, 349–350.
(51) Anson, F. C. *Anal. Chem.* **1966**, *38*, 54.

$(etpE)]_2(BF_4)_2$ is a chemically reversible process. Similar results were obtained for $[Pd(etp)]_2(BF_4)_2$ (see Experimental Section).

Mechanistic Studies. Role of Monodentate Phosphine Ligands. We have previously shown that $[Pd(etp)L](BF_4)_2$ complexes (where etp is bis[(diphenylphosphino)ethyl]phenylphosphine and L is a monodentate phosphine ligand or acetonitrile) catalyze the electrochemical reduction of CO_2 to CO in acidic *acetonitrile* solutions.[20,21] It was found that the catalytic current decreased as the concentration of the monodentate phosphine ligand increased. The precise step at which inhibition occurred was not determined. To investigate this point further, the ^{31}P NMR spectra of solutions of several complexes at acid concentrations identical to those used in catalytic experiments were examined. Figure 3 shows the ^{31}P NMR spectra of acetonitrile solutions of $[Pd(etp)(PEt_3)](BF_4)_2$ in the absence of acid (trace a) and in a 3×10^{-2} M HBF_4 solution (trace b). The resonance at 24.1 ppm in trace b corresponds to protonated triethylphosphine and the other resonances to $[Pd(etp)(CH_3CN)](BF_4)_2$. Similar behavior is observed when L is PPh_3 and $P(OMe)_3$. Catalytic currents are also observed in 3×10^{-2} M HBF_4 solutions when L is acetonitrile, PEt_3, PPh_3, and $P(OMe)_3$. Since the catalytic current and the peak potential of the catalytic wave are the same for complexes with different monodentate ligands, it is likely that the monodentate ligand dissociates to form a common species responsible for catalytic activity. No phosphine dissociation is observed for 3×10^{-2} M HBF_4 solutions of acetonitrile when L is $P(CH_2OH)_3$ or Ph_2PH, and no catalytic activity is evident at this concentration of HBF_4. At higher acid concentrations, these complexes become catalytic as reported previously.[20,21] In 3×10^{-2} M HBF_4 solutions of *dimethylformamide* or *acetone*, no monodentate phosphine dissociation can be detected by ^{31}P NMR spectroscopy for any of the $[Pd(etp)(PR_3)](BF_4)_2$ complexes and no catalysis is observed; however, $[Pd(etp)(CH_3CN)](BF_4)_2$ exhibits catalytic activity in these solvents. These experiments indicate that complexes containing monodentate phosphine ligands are catalyst precursors, but ligand dissociation must occur to form solvated complexes before the catalytic cycle can be entered. For this reason, our investigations of palladium complexes as catalysts have been restricted to complexes of the type [Pd(tridentate)(solvent)]$(BF_4)_2$ in which the fourth coordination site is occupied by a solvent molecule.

Electrochemical Studies of $[Pd(etpC)(DMF)](BPh_4)_2$ under Noncatalytic Conditions. Preliminary studies of the catalytic activities of a number of $[Pd(triphosphine)(CH_3CN)](BF_4)_2$ complexes indicated that the complex $[Pd(etpC)(CH_3CN)](BPh_4)_2$ (where etpC is bis[(dicyclohexylphosphino)ethyl]-phenylphosphine) in dimethylformamide would be suitable for further kinetic studies. This complex exhibits rates that are readily measurable by cyclic voltammetry, and it is less hygroscopic than other complexes. The catalytic reduction of CO_2 to CO involves both CO_2 and acid as substrates. Therefore, it is useful to examine the electrochemical behavior of $[Pd(etpC)(DMF)](BPh_4)_2$ in dimethylformamide in the presence of each substrate alone. The cyclic voltammogram of $[Pd(etpC)(DMF)](BPh_4)_2$ under nitrogen is shown by the solid trace in Figure 4. This complex exhibits an irreversible cathodic wave at −1.36 V. Plots of i_p versus $\nu^{1/2}$ indicate that this wave is diffusion controlled between 50 and 500 mV/s. On the basis of cyclic voltammetry and chronocoulometric experiments identical to those described above for [Pd(etpE)-$(DMF)](BF_4)_2$, this wave is assigned to two closely spaced, one-electron reductions. Associated with the cathodic wave is an irreversible anodic wave at −0.99 V. The shape of this wave and the linear dependence of i_p on ν are consistent with a surface-confined species.[52]

In the presence of 620 mmHg of CO_2 (the dotted trace in Figure 4), two irreversible one-electron reduction waves are observed at −1.28 and −1.72 V. The wave at −1.28 V is assigned to the reduction of $[Pd(etpC)(DMF)]^{2+}$ to $[Pd(etpC)(DMF)]^{1+}$. The wave at −1.72 V is assigned to the reduction of [Pd(etpC)-

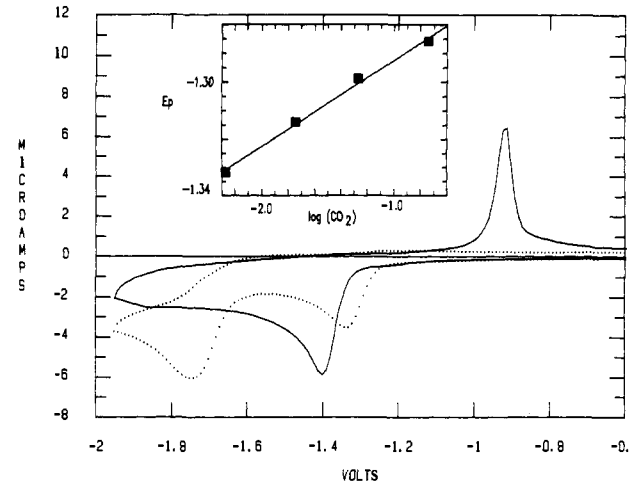

Figure 4. Cyclic voltammograms of 0.93×10^{-3} M solutions of [Pd-(etpC)(DMF)]$(BPh_4)_2$ (a) under nitrogen (solid line) and (b) after saturation with CO_2 at 620 mmHg (dotted line). The solutions were 0.3 N NEt_4BF_4 in dimethylformamide. The working electrode was glassy carbon, and the scan rate was 50 mV/s. The inset graph shows a plot of the peak potential of the first cathodic wave of [Pd(etpC)(DMF)]-$(BF_4)_2$ under CO_2 (dotted line) as a function of log $[CO_2]$.

$(DMF)(CO_2)]^+$. It can be seen from Figure 4 that the height of the cathodic wave observed for $[Pd(etpC)(DMF)]^{2+}$ under nitrogen (solid trace) decreases in the presence of CO_2 (dotted trace). This suggests that this wave has changed from one involving two closely spaced, one-electron reductions to a simple one-electron process. Chronoamperometric experiments were carried out in which the potential was stepped from −0.6 to −1.5 V across the first cathodic wave. The integrated Cotrell plots from this experiment gave a slope that is 0.54 times that observed under N_2 (supplementary Figure 1). This observation is consistent with the generation of a Pd(I) complex followed by reaction with CO_2, eq 7 and 8. As can be seen from Figure 4, the presence of CO_2

$$[Pd(etpC)(DMF)]^{2+} \overset{e^-}{\rightleftharpoons} [Pd(etpC)(DMF)]^{+} \quad (7)$$

$$[Pd(etpC)(DMF)]^{+} + CO_2 \xrightarrow{k} [Pd(etpC)(DMF)(CO_2)]^{+} \quad (8)$$

also results in a significant shift of the first wave to a more positive potential. For a reversible charge transfer followed by an irreversible reaction, the peak potential is expected to vary according to eq 9.[53] In eq 9, the rate constant k' is equal to $k[CO_2]$ under

$$E_p = E_{1/2} - \frac{RT}{nF}0.780 + \frac{RT}{2nF}\ln\frac{k'RT}{\nu nF} \quad (9)$$

pseudo-first-order conditions where $[CO_2] \gg$ [complex]. E_p should vary linearly with log $[CO_2]$ with a slope of 29 mV/decade change in CO_2 concentration at 21 °C. A plot of E_p versus log $[CO_2]$, shown in the inset of Figure 4, has a slope of 30 ± 5 mV. A plot of E_p versus log ν is also expected to have a slope of 29 mV from eq 9. The observed slope is 27 ± 5 mV for scan rates between 20 and 400 mV/s. If the reaction of $[Pd(etpC)(DMF)]^+$ with CO_2 is first order in $[Pd(etpC)(DMF)]^+$, the peak potential should be independent of the concentration of [Pd(etpC)-$(DMF)]^{2+}$. If the reaction is second order in complex, a plot of the peak potential versus the log of the complex concentration should exhibit a slope of 20 mV.[53] Experimentally the peak potential is found to be independent of the concentration of $[Pd(etpC)(DMF)]^{2+}$ between 4×10^{-4} and 4×10^{-3} M (supplementary Figure 2). These results are consistent with a reversible one-electron process followed by an irreversible reaction that is first order in CO_2 and complex as shown in eqs 7 and 8. Using eq 9 and an $E_{1/2}$ value of −1.283 V for the Pd(II/I) couple, a value of 42 M^{-1} s^{-1} can be calculated for the second-order rate constant,

(52) Bard, A. J.; Faulkner, L. R. *Electrochemical Methods*; Wiley: New York, 1980; pp 521–530.

(53) Nicholson, R. S.; Shain, I. *Anal. Chem.* **1964**, *36*, 706.

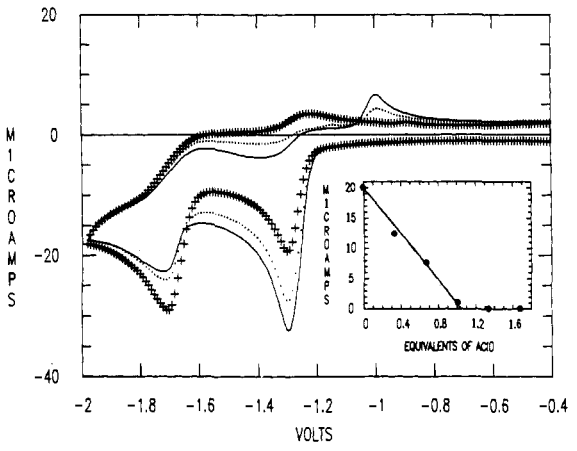

Figure 5. Cyclic voltammograms of 2.8×10^{-3} M [Pd(etpC)(DMF)]$(BF_4)_2$ in a DMF solution containing 0.18 M CO_2 and (a) no HBF_4 (+++ line), (b) 0.94×10^{-3} M HBF_4 (dotted line), and (c) 1.88×10^{-3} M HBF_4 (solid line). The inset graph is a plot of the peak current of the second cathodic wave versus the number of equivalents of acid added.

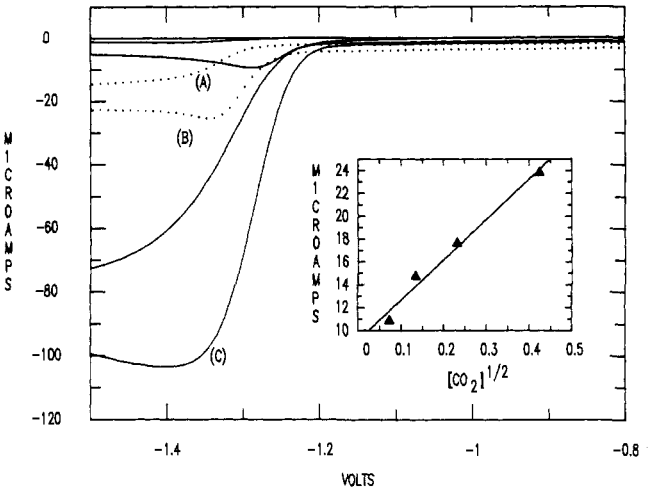

Figure 6. Cyclic voltammograms of 0.93×10^{-3} M solutions of [Pd(etpC)(DMF)]$(BPh_4)_2$ in DMF containing (A) 0.18 M CO_2 (solid line), (B) 4.7×10^{-2} M HBF_4 (dotted line), and (C) 0.18 M CO_2 and 4.7×10^{-2} M HBF_4 (solid line). The working electrode was glassy carbon, and the scan rate was 50 mV/s. The inset graph shows a plot of the observed catalytic current versus the $[CO_2]^{1/2}$ for a 2.0×10^{-4} M solution of [Pd(etpC)(DMF)]$(BPh_4)_2$ (3.8×10^{-2} M HBF_4 in DMF).

k, of reaction 8. The $E_{1/2}$ value of the Pd(II/I) couple was determined from the half-wave potential of the catalytic wave for CO_2 reduction (vide infra). Under catalytic conditions, $E_{p/2}$ is equal to $E_{1/2}$.[54] Due to the uncertainties involved in measuring peak and half-wave potentials ($\sim$5 mV), the uncertainty in the rate constant is $\pm$20.

Since the catalytic rate is much lower in dimethyl sulfoxide than in dimethylformamide (as discussed below), the effect of dimethyl sulfoxide on reaction 8 was examined. In dimethyl sulfoxide, the peak potential, E_p, varies linearly with log $[CO_2]$ and log ν with slopes of 22 $\pm$ 10 and 26 $\pm$ 10 mV, respectively. These results are consistent with reactions 7 and 8 as discussed for dimethylformamide solutions. In dimethyl sulfoxide, the reduction wave observed for [Pd(etpC)(DMSO)]$^{2+}$ under nitrogen is quasi-reversible (ΔE_p = 67 mV at 1 V/s), permitting a half-wave potential to be measured. The $E_{1/2}$ value obtained is -1.320 V and reflects an average value for the II/I and I/0 couples. If this value is used as an estimate of the Pd(II/I) couple, a second-order rate constant of 1.5×10^3 M^{-1} s^{-1} is obtained. Due to the uncertainties of estimating $E_{1/2}$ for the Pd(II/I) couple, this value must be regarded as providing an order-of-magnitude estimate. Even with this uncertainty, the rate of reaction of [Pd(etpC)(DMSO)]$^+$ with CO_2 is as fast or faster than the corresponding dimethylformamide complex shown in eq 8. The low catalytic rate observed in dimethyl sulfoxide is not due to a slow reaction of [Pd(etpC)(DMSO)]$^+$ with CO_2.

If small amounts of acid (less than 1 equiv/mol of catalyst) are added to DMF solutions of [Pt(etpC)(DMF)]$(BPh_4)_2$ under CO_2, the wave at -1.28 V increases in height while the wave at -1.72 V decreases in height as shown in Figure 5. This result suggests that [Pd(etpC)(DMF)(CO_2)]$^+$ is rapidly protonated in the presence of small amounts of HBF_4. The wave at -1.72 V decreases since [Pt(etpC)(DMF)(CO_2)]$^+$ is protonated before it can be reduced. A plot of the peak current for this wave versus the number of equivalents of acid per mole of catalyst is shown in the inset of Figure 5. The observation of a sharp end point at a 1:1 ratio is consistent with a single protonation of [Pd(etpC)(DMF)(CO_2)]$^+$. The resulting product [Pd(etpC)(DMF)(COOH)]$^{2+}$ undergoes a second reduction at potentials more positive than that of [Pd(etpC)(DMF)]$^{2+}$. This would account for the 2-fold increase in current for the wave at -1.28 V after the addition of 1 equiv of acid. These results are consistent with an ECCE but not with an ECEC mechanism.

Electrochemical and Kinetic Studies under Catalytic Conditions. Cyclic voltammograms of [Pd(etpC)(DMF)]$(BPh_4)_2$ in the presence of CO_2 (trace A), HBF_4 (trace B), and both CO_2 and HBF_4 (trace C) are shown in Figure 6. Comparison of curve C with curves A and B shows that in DMF solutions containing both acid and CO_2 a large catalytic wave for CO_2 reduction is observed with a half-wave potential of -1.283 V. For a reversible electron-transfer reaction followed by a fast catalytic reaction, i.e., an E_RC_{cat} scheme, the catalytic current is given by eq 10.[54]

$$i_c = nFA[\text{cat}](Dk[Q]^y)^{1/2} \quad (10)$$

The derivation of eq 10 assumes that the reaction is first order in catalyst and that the concentrations of the substrates, Q, are large compared to the concentration of the catalyst so that pseudo-first-order kinetics apply. From this equation, it can be seen that a plot of current versus the square root of the substrate should be linear if the reaction is first order in substrate. The inset graph in Figure 6 shows the linear plot obtained when the current is plotted versus the square root of the CO_2 concentration. This implies that the catalytic reaction is first order in CO_2 at these high acid concentrations. From eq 10, it can be seen that the catalytic current should have a linear dependence on the catalyst concentration for a reaction that is first order in catalyst. A plot of the catalytic current versus the concentration of [Pd(etpC)(DMF)]$(BPh_4)_2$ is linear between 1.0×10^{-4} and 1.0×10^{-3} M for CO_2 and HBF_4 concentrations of 0.18 and 3.84×10^{-2} M, respectively (supplementary Figure 3). In summary, at high acid concentrations the reaction is first order in both CO_2 and catalyst. These results are consistent with the reaction of [Pd(etpC)(DMF)]$^+$ with CO_2 being the rate-determining step at high acid concentrations as shown in reaction 8.

The dependence of the current on acid concentration in the presence of 0.18 M CO_2 is shown in Figure 7, trace C. At low acid concentrations, the current shows a linear dependence on acid concentration, while at higher concentrations the current reaches a limiting value that is independent of acid concentration. This behavior is typical of saturation kinetics expected for catalytic reactions.[55] The linear dependence of the current on acid at low concentrations, i.e., below 1.0×10^{-2} M, indicates a second-order dependence of the reaction rate on acid as shown in eq 10. Plots of current versus catalyst concentration are linear for solutions containing 3.8×10^{-3} M HBF_4 and 0.18 M CO_2 (supplementary Figure 4). This is consistent with a first-order dependence of the catalytic reaction on catalyst concentration. The current for 3.8×10^{-3} M HBF_4 solutions is independent of the CO_2 concentration from 1.8×10^{-2} to 1.8×10^{-1} M (supplementary Figure 5). This implies a zero-order dependence of the catalytic reaction on the

(54) Saveant, J. M.; Vianello, E. *Electrochim. Acta* **1963**, *8*, 905.

(55) Espenson, J. H. *Chemical Kinetics and Reaction Mechanisms*; McGraw-Hill: New York, 1981; pp 80–83.

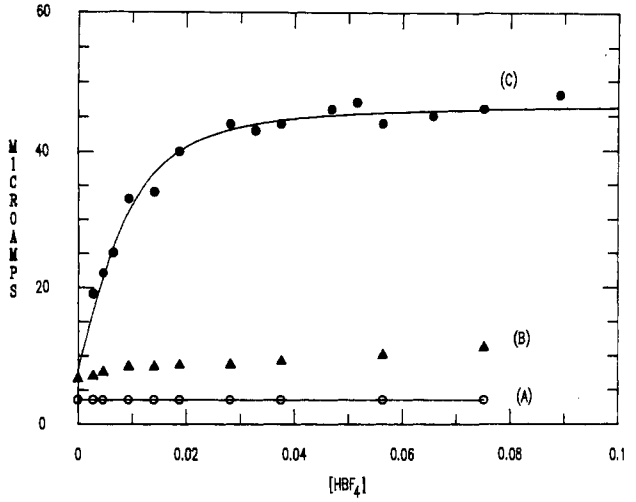

Figure 7. (A) Peak current observed for a solution containing 4.14×10^{-4} M catalyst and 0.18 M CO_2 but no acid. (B) Current observed for the same solution under nitrogen as a function of acid concentration. (C) Solid circles, peak current observed by cyclic voltammetry for a 4.14×10^{-4} M solution of $[Pd(etpC)(DMF)](BPh_4)_2$ in DMF containing 0.18 M CO_2 as a function of acid concentration; solid line, calculated as described in the text.

CO_2 concentration at low acid concentrations.

In summary, two kinetic regimes are observed depending on acid concentration. At high acid concentration, the rate of CO_2 reduction is first order in catalyst, first order in CO_2, and independent of acid. At low acid concentrations, the reaction is first order in catalyst, second order in acid, and independent of the CO_2 concentration. This is consistent with a change in the rate-determining step on going from low to high acid concentrations.

Figure 6, trace B, shows the cyclic voltammogram of $[Pd(etpC)(CH_3CN)](BPh_4)_2$ in the presence of acid under nitrogen, i.e., no CO_2 present. A catalytic wave is observed with the half-wave potential equal to −1.32 V. The product of the catalytic reaction is hydrogen as verified by gas chromatography (current efficiency 104%). The observation that the half-wave potential is approximately 40 mV negative of the half-wave potential for CO_2 reduction suggests that a Pd(0) species is required for proton reduction while a Pd(I) species reacts with CO_2. The catalytic current also shows a small linear dependence on acid concentration as shown in Figure 7, trace B. This implies a second-order dependence of the catalytic rate for H_2 production on the concentration of HBF_4 (eq 10). A plot of the catalytic current observed for proton reduction versus the concentration of $[Pd(etpC)(DMF)](BPh_4)_2$ is linear. This is consistent with a first-order dependence on catalyst. To summarize, the rate of hydrogen production is first order in $[Pd(etpC)(DMF)(BF_4)_2$ and second order in HBF_4 and appears to involve a Pd(0) intermediate.

Equation 11 shows the parameters determining the peak current of a compound with a reversible electron transfer and no following reaction.[49] It can be seen from a comparison of eqs 10, which describes the catalytic case, and 11 that the ratio of i_c to i_p permits calculation of the catalytic rate constant, k, in eq 10. (When

$$i_p = 0.446n^{3/2}FA[\text{cat}](F/RT)^{1/2}\nu^{1/2}D^{1/2} \qquad (11)$$

the ratio of i_c to i_p is less than 2.0, the catalytic rate constants can be evaluated using working curves developed by Nicholson and Shain.[53]) The values for i_c were obtained by subtracting the current observed when only acid is present from the total current observed when both CO_2 and acid are present ($i_c = i_{CO_2+H^+} - i_{H^+}$, trace C − trace B of Figure 7). Since the reduction of CO_2 to CO requires two electrons, the value of n for eq 10 is 2. For $[Pd(etpC)(DMF)](BF_4)_2$, the peak current for the first wave under CO_2 in Figure 4, i_p, corresponds to a one-electron reduction as discussed above, and the value of n to be used in eq 11 is 1. The magnitude of this current is shown by trace A of Figure 7. After correcting for the background hydrogen reduction and different

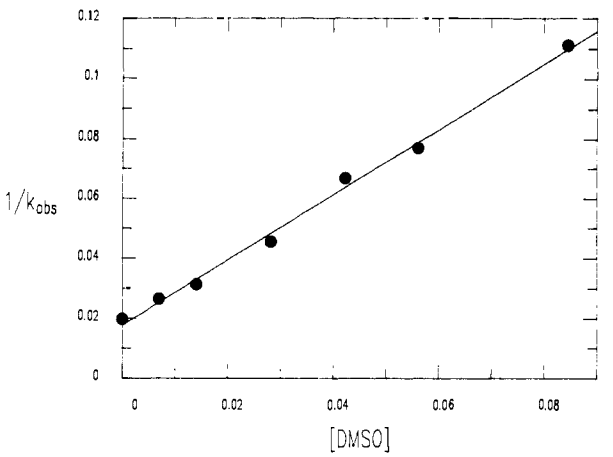

Figure 8. $1/k_{obsd}$ versus the concentration of dimethyl sulfoxide in dimethylformamide (0.18 M CO_2, 1.0×10^{-3} M $[Pd(etpC)(DMF)](BPh_4)_2$, 4.7×10^{-2} M HBF_4).

Table IV. Electrochemical and Catalytic Data for $[Pd(tridentate)(DMF)](BF_4)_2$ Complexes in Dimethylformamide

tridentate ligand	$E_{1/2}$, V[a]	k, M^{-1} s^{-1}	current efficiency, % CO	current efficiency, % H_2	turnover[c] number
MetpC	−1.45	160 ± 35	13	90	11 (87)
MetpE	−1.47	180 ± 35	10	90	4 (40)
etpC	−1.28	50 ± 20	85	16	130 (154)
etpE	−1.25	40 ± 15	65	37	10 (15)
BetpE	−1.30	25 ± 10	77	23	13 (17)
etp	−1.11	13 ± 7	54	48	45 (86)
BetpN	−1.22	4 ± 2	9	85	3 (31)
NetpN	−1.25	5 ± 2	21	74	4 (18)
ttp	−1.12	<1	2	100	2 (102)
CttpM, **2**	−1.44[b]	<1			
PPS, **3**	−1.01[b]	<1			
PPy_2, **4**	−1.32[b]	<1			
terpy	−1.00[b]	<1			

[a] All potentials are given versus ferrocene as an internal standard. [b] Reduction waves are irreversible, and potentials are given for the peak current of the first cathodic wave. [c] The turnover number is calculated on the basis of the number of moles of CO produced per mole of catalyst. The values in parentheses are calculated on the basis of the total moles of CO and H_2 produced per mole of catalyst.

n values, a second-order rate constant of 53 (±20) M^{-1} s^{-1} at 21 °C is obtained. This value is within experimental error of the value derived from the shift in the peak potential of $[Pd(etpC)(DMF)](BPh_4)_2$ in the presence of CO_2 (vide supra). Chronoamperometric methods also give the same value, $k = 50$ M^{-1} s^{-1}.[56] If no correction is applied for hydrogen current, i_{H^+}, the observed rate constant increases to 70 M^{-1} s^{-1}. The same approach can be used to derive a value of $(6 \pm 4) \times 10^4$ M^{-2} s^{-1} for the third-order rate constant for the reaction of H^+ with the catalyst–CO_2 complex observed at low acid concentrations (first linear regime of Figure 7).

Influence of Solvent and CO on Catalytic Activity. The rate constants obtained for the catalytic reduction of CO_2 to CO at high acid concentrations in acetonitrile, dimethylformamide, and dimethyl sulfoxide are 200 ± 100, 50 ± 20, and less than 1 M^{-1} s^{-1}, respectively. The origin of the low rates in dimethyl sulfoxide was investigated by adding small amounts of dimethyl sulfoxide to dimethylformamide solutions containing CO_2, HBF_4, and catalyst. Figure 8 shows a plot of one over the observed rate constant versus the concentration of dimethyl sulfoxide. The linear plot is consistent with dimethyl sulfoxide acting as a linear inhibitor of the catalyst.[57,58] Although CO might be expected to inhibit

(56) Delahay, P.; Steihl, G. L. *J. Am. Chem. Soc.* **1952**, *74*, 3500. Bard, A. J.; Faulkner, L. R. *Electrochemical Methods*; Wiley: New York, 1980; pp 456–457.

(57) Huang, C. Y. In *Contemporary Enzyme Kinetics and Mechanism*, Purich, D. L., Ed.; Academic Press: New York, 1983; p 1.

the catalytic reduction of CO_2, no inhibition was observed for gas mixtures of CO_2 and CO containing 30% CO (supplementary Figure 6).

Influence of the Tridentate Ligand. Table IV shows the rate constants obtained for the reaction of $[Pd(triphosphine)(DMF)]^+$ with CO_2 at high acid concentrations. It can be seen that the nature of the tridentate ligand has a major influence on this rate. Comparison of the rate constants of $[Pd(MetpC)(CH_3CN)](BF_4)_2$ with $[Pd(MetpE)(CH_3CN)](BF_4)_2$ and $[Pd(etpC)(CH_3CN)](BPh_4)_2$ with $[Pd(etpE)(CH_3CN)](BF_4)_2$ indicates that the steric bulk of R', the substituent on the terminal phosphorus atoms of the triphosphine ligand, has little effect on the rate. Comparison of the rate constants of $[Pd(etpC)(CH_3CN)](BPh_4)_2$ and $[Pd(etpE)(CH_3CN)](BF_4)_2$ with $[Pd(etp)(CH_3CN)](BF_4)_2$ shows that more electron-rich alkyl groups promote the reaction. Electronic effects of the substituents on the terminal phosphorus atoms appear to be more important than steric effects. Comparison of the rate constants of $[Pd(MetpE)(CH_3CN)](BF_4)_2$, $[Pd(etpE)(CH_3CN)](BF_4)_2$, and $[Pd(BetpE)(CH_3CN)](BF_4)_2$ shows that the rate constant decreases as the steric bulk of the substituent on the central phosphorus atom increases. Electronic effects on the central phosphorus atom appear to be of secondary importance compared to steric effects. Comparison of the rate constants of $[Pd(ttp)(CH_3CN)](BF_4)_2$ with $[Pd(etp)(CH_3CN)](BF_4)_2$ shows that the bite size of the triphosphine ligand exerts a significant effect on the rate. Finally, all complexes that contain donor atoms other than phosphorus in the tridentate ligand are not catalytically active.

The influence of the tridentate ligand was also investigated by controlled potential electrolysis. In these experiments, the catalytic solutions were exhaustively electrolyzed, and the amounts of H_2 and CO formed were analyzed by gas chromatography. These results were used to calculate current efficiencies for these products as shown in Table IV. It can be seen that the total charge passed can be accounted for by the formation of hydrogen and carbon monoxide. The combined error in the current efficiencies is estimated to be ±5%. Turnover numbers for the catalysts under conditions described in the Experimental Section are also shown in Table IV. The conditions were not optimized. In those cases where the major metal-containing decomposition products were conclusively identified (see Experimental Section and supplementary material), they were triphosphine-bridged metal dimers similar to that shown in Figure 1. The electrolysis experiments also provide information on the selectivity and current efficiencies of the various catalysts.

Discussion

Synthesis. The ^{31}P NMR spectral studies and electrochemical studies described for $[Pd(etp)(PR_3)](BF_4)_2$ complexes in acidic acetonitrile solutions show that these complexes are precursors to the actual catalyst $[Pd(etp)(CH_3CN)](BF_4)_2$. This conclusion suggests that the synthesis of a variety of complexes of the type $[Pd(tridentate)(solvent)](BF_4)_2$ could provide information on the relationship between structure and reactivity for this class of catalysts. The reactions used to prepare the various tridentate ligands needed for such a study are shown in reactions 1–4. These ligands permit a systematic variation of steric factors, phosphine basicity, chelate chain length, and heteroatom donors. Reaction of these tridentate ligands with $[Pd(CH_3CN)_4](BF_4)_2$ provides a direct route to $[Pd(tridentate)(CH_3CN)](BF_4)_2$ complexes. The lability of the coordinated acetonitrile in these complexes permits facile conversion to $[Pd(tridentate)L](BF_4)_2$ complexes where L can be other solvent molecules, phosphines, or halide ions.

Mechanism of CO_2 Reduction. Kinetic and electrochemical studies were carried out on $[Pd(etpC)(DMF)](BPh_4)_2$ complexes to gain insight into the mechanistic features of the reduction of CO_2 to CO catalyzed by $[Pd(triphosphine)(solvent)](BF_4)_2$ complexes. We believe that the mechanism shown in Scheme I accounts for the kinetic and electrochemical results described.

Scheme I

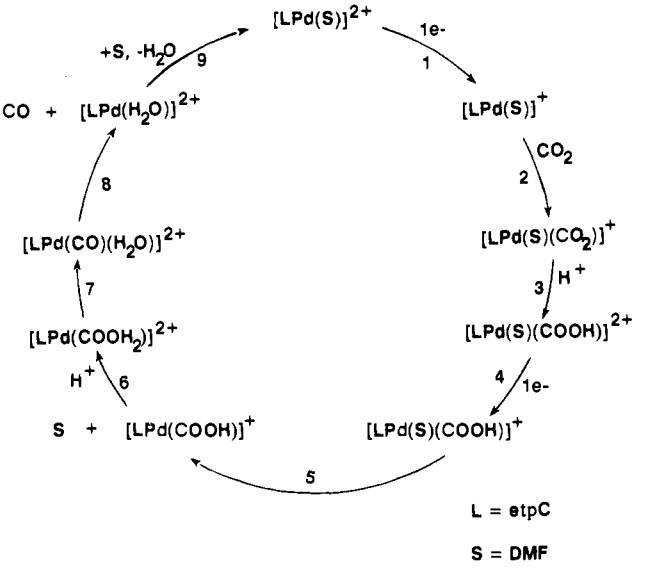

Using $[Pd(etpC)(DMF)]^{2+}$ as a starting point, it is reasonable to propose that the first two steps in the catalytic cycle are the one-electron reduction of $[Pd(etpC)(DMF)]^{2+}$ followed by reaction with CO_2 as shown in Scheme I. A one-electron process is supported by comparison of cyclic voltammograms of $[Pd(etpC)(DMF)]^{2+}$ under nitrogen and CO_2 (Figure 4, solid and dotted traces, respectively), the slopes of the charge versus $t^{1/2}$ plots for potential step experiments (supplementary Figure 1), and the 30 mV/decade dependence of E_p on the CO_2 concentration as shown in the inset graph of Figure 4. In the presence of CO_2 and absence of acid, the palladium(I) complex $[Pd(etpC)(DMF)]^+$ reacts rapidly with CO_2 to form $[Pd(etpC)(DMF)(CO_2)]^+$ in a reaction that is first order in CO_2 and first order in $[Pd(etpC)(DMF)]^+$ (step 2 of Scheme I). At high acid concentrations, this reaction appears to be the rate-determining step in the catalytic cycle, since the rate of CO_2 reduction is also first order in catalyst and first order in CO_2 (Figure 6 and supplementary Figure 3). The observed second-order rate constants for the stoichiometric and catalytic reactions (42 and 53 M^{-1} s^{-1}, respectively) are the same within experimental error. The close agreement between these rate constants suggests that the same reaction is rate determining in both processes. Further support for this interpretation comes from a comparison of the rate constants determined for the stoichiometric reaction of $[Pd(NetpN)(DMF)]$ with CO_2 (4 M^{-1} s^{-1}) with the catalytic rate constant (5 M^{-1} s^{-1}).[60]

The next step following formation of $[Pd(etpC)(DMF)(CO_2)]^+$ is a chemical step and not an electron transfer. The potential at which the catalytic wave is observed corresponds to the potential at which $[Pd(etpC)(DMF)]^{2+}$ is reduced (−1.28 V). This indicates that during the catalytic cycle a second electron transfer occurs at a potential positive of −1.28 V. Thus, the potential at which the catalytic wave occurs is not consistent with reduction of $[Pd(etpC)(DMF)(CO_2)]^+$ (−1.7 V). This rules out an ECE mechanism. In DMF solutions, protonation of $[Pd(etpC)(DMF)(CO_2)]^+$ appears to be the next step, step 3 of Scheme I. As seen in Figure 5, the effect of small quantities of acid on the cyclic voltammogram of $[Pd(etpC)(DMF)]^{2+}$ in the presence of CO_2 is to decrease the wave at −1.7 V and increase the catalytic wave at −1.28 V. The 1:1 stoichiometry of acid to complex indicated by the titration curve shown in the inset of Figure 5 is consistent with the protonation shown in step 3.

The precise sequence of steps following the protonation of $[Pd(etpC)(DMF)(CO_2)]^+$ is ambiguous. A second electron transfer (step 4 of Scheme I) must occur during the catalytic cycle in order to produce CO. The source of the second electron may be either the electrode of $[Pd(etpC)(DMF)]^+$. Although the

(58) King, E. L.; Altman, C. *J. Phys. Chem.* **1956**, *60*, 1375.
(59) March, J. *Advanced Organic Chemistry*; McGraw Hill: New York, 1968; pp 219–220.
(60) DuBois, D. L. Unpublished results.

Scheme II

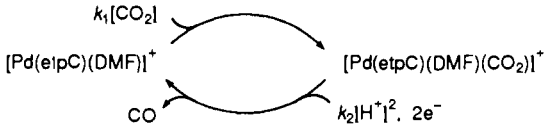

placement of step 4 represents a reasonable sequence, it has not been proven. The inclusion of step 5 in the mechanism is based on the observation that dimethyl sulfoxide acts as a reversible linear inhibitor of the catalytic reaction (Figure 8). Studies of the rate of reaction of [Pd(etpC)(DMSO)]$^+$ with CO_2 in dimethyl sulfoxide show that this reaction is fast even though no catalytic reaction is observed in this solvent. Therefore, the inhibition is not due to a competitive inhibition of the reaction with CO_2. The inhibition is also too large to attribute to normal solvation effects. Since dimethyl sulfoxide is intermediate in basicity compared with acetonitrile and dimethylformamide,[59] it is unlikely that a decrease in proton activity is responsible for the inhibition. Also, low concentrations of DMSO relative to the concentration of HBF_4 still produce significant inhibition. At high acid concentrations, the removal of a small fraction of available protons by a base should not result in a decrease in catalyst activity (Figure 7). A reasonable explanation of the decreased catalytic rate is that the solvent molecule originally in the coordination sphere of the catalyst must be lost for the catalytic cycle to occur as shown in step 5. When the solvent is dimethylformamide or acetonitrile, the loss of solvent is facile. When the solvent is dimethyl sulfoxide, the loss of solvent is unfavorable and inhibits further reaction. That dimethyl sulfoxide binds more strongly to palladium in the +2 oxidation state is shown by the displacement of dimethylformamide and acetonitrile from [Pd(etpC)(solvent)]$(BPh_4)_2$ as observed by ^{1}H NMR spectroscopy. The more reversible reduction of [Pd(etpC)(DMSO)]$(BPh_4)_2$ compared to [Pd(etpC)-(CH_3CN)]$(BPh_4)_2$ and [Pd(etpC)(DMF)]$(BPh_4)_2$ indicates that dimethyl sulfoxide binds more strongly to palladium(0) as well. The importance of ligand loss is also supported by the observation that complexes of the type [Pd(triphosphine)(PR_3)]$(BF_4)_2$ are catalytically inactive unless the monodentate PR_3 ligand is lost by protonation. Also, no complexes of the type [Pd(diphos)$_2$]-$(BF_4)_2$ are catalytically active. The palladium(0) complexes of the latter two classes can react directly with CO_2, however. The vacant coordination site produced by solvent loss may be filled by an oxygen atom of CO_2. This would result in the formation of an η^2 complex. If this interpretation of the origin of the catalyst inhibition by DMSO is correct, it suggests that the formation of an η^2 CO_2 fragment is required for cleavage of the carbon–oxygen bond shown in step 7. Alternatively, the loss of solvent may simply be required to produce the proper electronic environment for cleavage of the carbon–oxygen bond.

The second-order dependence of the catalytic rate on acid concentration at low acid concentrations is consistent with the reaction of the CO_2 complex with two protons as shown in steps 3 and 6. The proton dependence coupled with the requirement for solvent loss suggests that the composition of the activated complex at low acid concentrations is [Pd(etpC)($COOH_2$)]$^{2+}$. However, the precise sequence of protonation, electron transfer, and solvent loss (steps 3–6) required to produce the activated complex is not known and may vary with solvent and catalyst. A reasonable rate-determining step at low acid concentrations would be the cleavage of the carbon–oxygen bond, step 7. The subsequent steps of CO loss and displacement of water by solvent are needed to complete the catalytic cycle. If the loss of CO, step 8, is reversible, or if CO binding to the Pd(I) intermediate were competitive with CO_2 binding, then CO should inhibit the rate of CO_2 reduction. Such an inhibition is not observed as shown in Figure 6 of the supplementary material.

The mechanism shown in Scheme I is based on a combination of spectroscopic, electrochemical, and kinetic measurements carried out under various conditions. For the purposes of kinetic analysis, Scheme I can be simplified to Scheme II which undoubtedly omits a number of chemically important (but not rate-determining) steps. The rate equation for this cycle is shown by eq 12,[57,58] where E_o is the total concentration of [Pd(etpC)(DMF)]$(BPh_4)_2$. Equation 12 reduces to eqs 13 and 14 at high and low acid concentrations, respectively. These limiting forms are consistent with our experimental observations of a first-order dependence on CO_2 at high acid concentrations and a second-order dependence on acid at low acid concentrations. If the rate expression shown in eq 12 is substituted into eq 10 and corrections are made for the background H_2 current as described above, the solid line shown in Figure 7 can be calculated for a k_1 value of 53 and a k_2 value of 6×10^4.

$$\frac{d[CO]}{dt} = \frac{k_1 k_2 [CO_2][H^+]^2 E_o}{k_1[CO_2] + k_2[H^+]^2} \quad (12)$$

$$\frac{d[CO]}{dt} = k_1[CO_2]E_o \quad (13)$$

$$\frac{d[CO]}{dt} = k_2[H^+]^2 E_o \quad (14)$$

For a second-order reaction of the reduced catalyst with CO_2, it is expected that increasing the electron density on the catalyst would increase the observed rate constant. Increasing the steric requirements of the complex should decrease the observed rate constant. As the electron-donating abilities of the substituents on the terminal phosphorus atoms increase (and $E_{1/2}$ becomes more negative), the rate of reaction with CO_2 increases as shown in Table IV. Three of the complexes that are out of sequence, [Pd(BetpE)(DMF)]$(BF_4)_2$, [Pd(NeptN)(DMF)]$(BF_4)_2$, and [Pd(BetpN)(DMF)]$(BF_4)_2$, are also severely crowded due to the bulkiness of the substituents. The steric bulkiness of these complexes may account for their lower reactivity. The observation that [Pd(ttp)(DMF)]$(BF_4)_2$ is a much slower catalyst than [Pd(etp)(DMF)]$(BF_4)_2$ is interesting. These two complexes have approximately the same redox potential, and the steric and electronic requirements for the ligand substituents are identical. The only structural difference between these complexes is the bite size of the triphosphine ligand. A three-carbon chain is present in ttp, and a two-carbon chain is present in etp. It could be argued that the greater ring strain for the etp complex promotes dissociation of one of the terminal phosphorus atoms of the tridentate ligand, which promotes reactivity. If this were true, the complexes [Pd(dppp)(CH_3CN)$_2$]$(BF_4)_2$ and [Pd(dppp)(PEt_3)$_2$]$(BF_4)_2$ (where dppp is bis(diphenylphosphino)propane)[61] should be better catalysts than either triphosphine ligand since they can readily dissociate a monodentate ligand. Neither complex exhibits detectable catalytic activity, however. A more likely explanation for the difference in reactivity between [Pd(etp)(DMF)]$(BF_4)_2$ and [Pd(ttp)(DMF)]$(BF_4)_2$ is that ligands containing two-carbon chains promote planarity for the +1 oxidation state.[61] A more planar structure results in a higher energy d_{z^2} orbital perpendicular to the plane of the molecule. This filled orbital interacts directly with the incoming CO_2 ligand.

Side Reactions. The last two columns of Table IV list the results of controlled potential electrolysis studies of the various catalysts prepared in this study. Two points regarding the turnover numbers deserve comment. First, the catalysts studied to date are rather fragile, with low turnover numbers. Second, of the four catalysts showing the highest turnover numbers ([Pd(etpC)(DMF)]$(BFh_4)_2$, [Pd(etpE)(DMF)]$(BF_4)_2$, [Pd(BetpE)(DMF)]$(BF_4)_2$, and [Pd-(etp)(DMF)]$(BF_4)_2$), increasing the steric bulk of the substituents on the terminal phosphorus atoms increases the turnover numbers. That [Pd(etpC)(DMF)]$(BPh_4)_2$ would have a longer catalyst lifetime than [Pd(etp)(DMF)]$(BF_4)_2$, [Pd(BetpE)(DMF)]$(BF_4)_2$, and [Pd(etpE)(DMF)]$(BF_4)_2$ is expected. The etpC ligand has the bulkiest terminal substituents, which should retard the formation of dimers analogous to the structurally characterized [Pt(etp)]$_2(BF_4)_2$ and [Pd(etpE)]$_2(BF_4)_2$ complexes. These dimers are the major metal-containing products observed after exhaustive electrolysis of catalytic solutions. The observation that the triphosphine-bridged dimers can be reoxidized to generate the or-

(61) Miedaner, A.; DuBois, D. L. *Inorg. Chem.* **1991**, *30*, 417.

iginal catalysts indicates that deactivation is reversible. Other approaches to retarding the dimerization reactions will be examined in the future.

The controlled potential electrolysis experiments also provide information on the selectivities and current efficiencies of the various catalysts. Generally, the selectivity for carbon monoxide production roughly parallels the catalytic rate as shown in Table IV. As the rate constant for reaction with CO_2 increases, the current efficiency increases. This is consistent with a competitive reaction occurring for the [Pd(triphosphine)(DMF)]$^+$ intermediate. This intermediate can react with CO_2 (as shown in eq 8) and ultimately form CO. Alternatively, it can be reduced a second time at the electrode to form a Pd(0) complex, which is protonated and subsequently forms hydrogen as observed for [Pd(ttp)H]-$(BF_4)_2$. As the rate of reaction of the Pd(I) intermediate with CO_2 increases, the production of CO relative to hydrogen should increase. Increasing the concentration of CO_2 should favor formation of the Pd(I)CO_2 complex and increase the ratio of CO to hydrogen. For [Pd(etpC)(DMF)]$(BPh_4)_2$, the current efficiency at 620 mmHg of CO_2 is approximately 85% as shown in Table IV. At 62 mmHg, 9% of the current forms CO and the remainder produces hydrogen. This result is consistent with a competitive reaction for the Pd(I) intermediate. Surprisingly, however, the large rate constants observed for [Pd(MetpE)(DMF)]$(BF_4)_2$ and [Pd(MetpE)(DMF)]$(BF_4)_2$ do not result in high current efficiencies for CO production. In fact, low efficiencies (approximately 10%) are observed. We attribute this low efficiency to a new pathway for hydrogen production for these two complexes. This pathway proceeds through a [Pd(triphosphine)(DMF)-(CO_2)]$^+$ intermediate. The reason for invoking this CO_2 intermediate for hydrogen production is that the results of kinetic studies for [Pd(MetpC)(DMF)]$(BF_4)_2$ and [Pd(MetpE)-(DMF)]$(BF_4)_2$ are almost identical with those of [Pd(etpC)-(DMF)]$(BPh_4)_2$ described previously. For example, at low acid concentrations the catalytic current is proportional to catalyst concentration and acid concentration. At high acid concentrations, the catalytic current is proportional to the catalyst concentration and the square root of CO_2 concentration, but independent of acid concentrations. The observation that the catalytic current is dependent on CO_2 concentration implies that the rate of reaction of the Pd(I) species with CO_2 is still rate determining at high acid concentrations, even though the product in this case is hydrogen and not CO. Apparently, for [Pd(MetpC)(DMF)(CO_2)]$^+$ and [Pd(MetpE)(DMF)(CO_2)]$^+$ two pathways are available. One pathway results in hydrogen production, the other in CO production. The pathway followed may depend on the redox potential of the catalyst or the steric requirements of the substituents on the central phosphorus atoms of the triphosphine ligand. There are insufficient data at this point to determine precisely which factors are responsible for determining the selectivity. This aspect is under investigation. The results are that, as the reduction potential of the catalyst becomes more negative, the selectivity for CO first increases and then decreases. However, the rate constants for reaction of the [Pd(triphosphine)(DMF)]$^+$ complexes with CO_2 show a monotonic increase.

A second approach to increasing the selectivity is to decrease the rate of hydrogen production. One pathway for hydrogen production likely proceeds through hydride intermediates such as [Pd(etpC)H](BF_4) and [Pd(ttp)H](BF_4). The former can be detected spectroscopically while the latter can be isolated and characterized. These hydrides are formed by protonation of palladium(0) complexes, and under more acidic conditions they are protonated to form H_2. The half-wave potential for the catalytic production of hydrogen by [Pd(etpC)(DMF)]$(BPh_4)_2$ is negative of the half-wave potential for CO_2 reduction. This is consistent with the reduction of palladium(II) to palladium(I) for CO_2 reduction and palladium(I) to palladium(0) for hydrogen production. These results suggest that catalysts with a large separation between the (II/I) and (I/0) couples should be more selective. The observation that these hydrides do not react with CO_2 also eliminates the possibility of these palladium hydrides as catalytic intermediates as we have suggested previously.[20]

The mechanism and side reactions discussed above for [Pd-(etpC)(DMF)]$(BPh_4)_2$ have features in common with cobalt and nickel macrocycles reported by other researchers. For nickel macrocycles, CO_2 reacts rapidly with a Ni(I) species.[4-6,62,63] In this work, rapid reactions between CO_2 and Pd(I) intermediates are observed. The somewhat higher selectivity for CO relative to hydrogen observed for Ni(cyclam)$^{2+}$ compared to our catalysts under one atmosphere of CO_2 may arise in part from the larger separation between the Ni(II/I) and Ni(I/0) couples compared to the Pd(II/I) and Pd(I/0) couples. It has also been proposed that hydrogen bonding between an oxygen atom of coordinated CO_2 and a proton bound to nitrogen plays an important role in the catalytic reduction of CO_2 and in the binding of CO_2 to certain cobalt macrocycles.[4,5] This bifunctional activation appears to be similar to the η^2 bonding suggested above for [Pd(etp)COOH]$^{2+}$. In the former case, the C–O bond would be weakened by the binding between oxygen and a proton, and in the latter the formation of a palladium–oxygen bond may play a similar role.

Summary and Conclusions

The synthesis and screening of a variety of [Pd(tridentate)-(solvent)]$(BF_4)_2$ complexes show that the requirements for catalytic activity are stringent and require a triphosphine ligand and a solvent molecule in the coordination sphere. Heteroatom substitution in the triphosphine ligand results in loss of catalytic activity. Mechanistic studies indicate that the rate-determining step in the catalytic cycle at high acid concentrations is the reaction of a Pd(I) complex with CO_2. This reaction is promoted by electron-donating substituents on the triphosphine ligand and retarded by bulky substituents on the central phosphorus atom. This reaction is also faster for catalysts containing triphosphine ligands with two-carbon backbones than for those containing three-carbon backbones. The former presumably have a high-lying d_{z^2} orbital that promotes the reaction with CO_2.[61] At low acid concentrations, a second rate-determining reaction becomes operative; this reaction shows a second-order dependence on acid concentration. This result is consistent with the cleavage of a carbon–oxygen bond being rate determining. Inhibition of the catalytic reaction by DMSO suggests that loss of solvent may be required for catalytic activity. The majority of the catalysts are deactivated by formation of Pd(I) dimers, two of which have been structurally characterized. This deactivation can be reversed by electrochemical oxidation. Finally, the structure of the triphosphine ligand appears to exert a major influence over the selectivity of the catalysts, but a clear understanding of this relationship is not yet available.

Acknowledgment. This work was supported by the United States Department of Energy, Office of Basic Energy Sciences, Chemical Sciences Division.

Supplementary Material Available: Detailed preparations for all ligands and complexes described in this paper to enable reproduction of this work, Figures 1s–6s, containing electrochemical data described in the text, Tables 1s and 8s, containing crystal data, data collection conditions, and solution and refinement details for [Pd(etp)]$_2(BF_4)_2$ and [Pd(etpE)]$_2(BF_4)_2$, Figures 7s and 8s, showing diagrams with atom numbering schemes, and Tables 2s–6s and 9s–13s, listing atomic coordinates and equivalent isotropic displacement parameters, bond lengths, bond angles, anisotropic displacement parameters, and hydrogen atom coordinates and isotropic parameters (49 pages); Tables 7s and 14s, listing calculated and observed structure factors (59 pages). Ordering information is given on any current masthead page.

(62) Pearce, D. J.; Pletcher, D. *J. Electroanal. Chem. Interfacial Electrochem.* **1986**, *197*, 317.
(63) Fujihira, M.; Hirata, Y.; Suga, K. *J. Electroanal. Chem. Interfacial Electrochem.* **1990**, *292*, 199.